

Anomalous summertime CO₂ sink in the subpolar Southern Ocean promoted by early 2021 sea ice retreat

Kirtana Naëck^{1*}, Jacqueline Boutin¹, Sebastiaan Swart², Marcel du Plessis², Liliane Merlivat¹, Laurence Beaumont³, Antonio Lourenco¹, Francesco d'Ovidio¹, Louise Rousselet¹, Brian Ward⁴, Jean-Baptiste Sallée¹

¹ Sorbonne Université, CNRS, IRD, MNHN, Laboratoire d'Océanographie et du Climat : Expérimentations et Approches Numériques, LOCEAN/IPSL, F-75005 Paris, France

²Department of Marine Sciences, University of Gothenburg, Sweden

³DT-INSU Meudon, France

⁴University of Galway, Ireland

* Correspondence to: kirtana.naek@locean.ipsl.fr and jacqueline.boutin@locean.ipsl.fr

Abstract

The physical and biogeochemical processes governing the air-sea CO₂ flux in the Southern Ocean are still widely debated. The “Southern Ocean Carbon and Heat Impact on Climate” cruise in summer 2022 aimed at studying these processes in the Weddell Sea and in its vicinity. A “CARbon Interface Ocean Atmosphere” (CARIOCA) drifting buoy was deployed in January 2022 in the subpolar Southern Ocean, providing hourly surface ocean observations of fCO₂ (fugacity of CO₂), dissolved oxygen, salinity, temperature and chlorophyll-a fluorescence for 17 months. An underwater glider was piloted with the buoy for the first 6 weeks of the deployment to provide vertical ocean profiles of hydrography and biogeochemistry. These datasets reveal an anomalously strong ocean carbon sink for over 2 months ~~occurring~~ in the region of Bouvet Island and associated with large plumes of chlorophyll-a (Chl-a). Based on Lagrangian backward trajectories reconstructed using various surface currents fields, we identified that the water mass reaching the Bouvet Island region originated from the south-west, from the vicinity of sea ice edge in spring 2021. ~~We suggest that a~~ strong phytoplankton bloom developed there in November 2021 ~~through dissolved iron supplied. We propose that it was promoted~~ by early sea ice ~~melt~~retreat in 2021 in the Weddell Sea. These waters, depleted in carbon, then travelled to the position of the CARIOCA buoy. The very low values of ocean fCO₂, measured by the buoy (down to 310 µatm), are consistent with net community production previously observed during blooms occurring near the sea ice edge, partly compensated by air-sea CO₂ flux along the water mass trajectory. Early sea ice retreat might therefore have caused a large CO₂ sink farther north than usual in summer 2022, in the Atlantic sector of the subpolar Southern Ocean. Such events might become more frequent in the future as a result of climate change.

1. Introduction

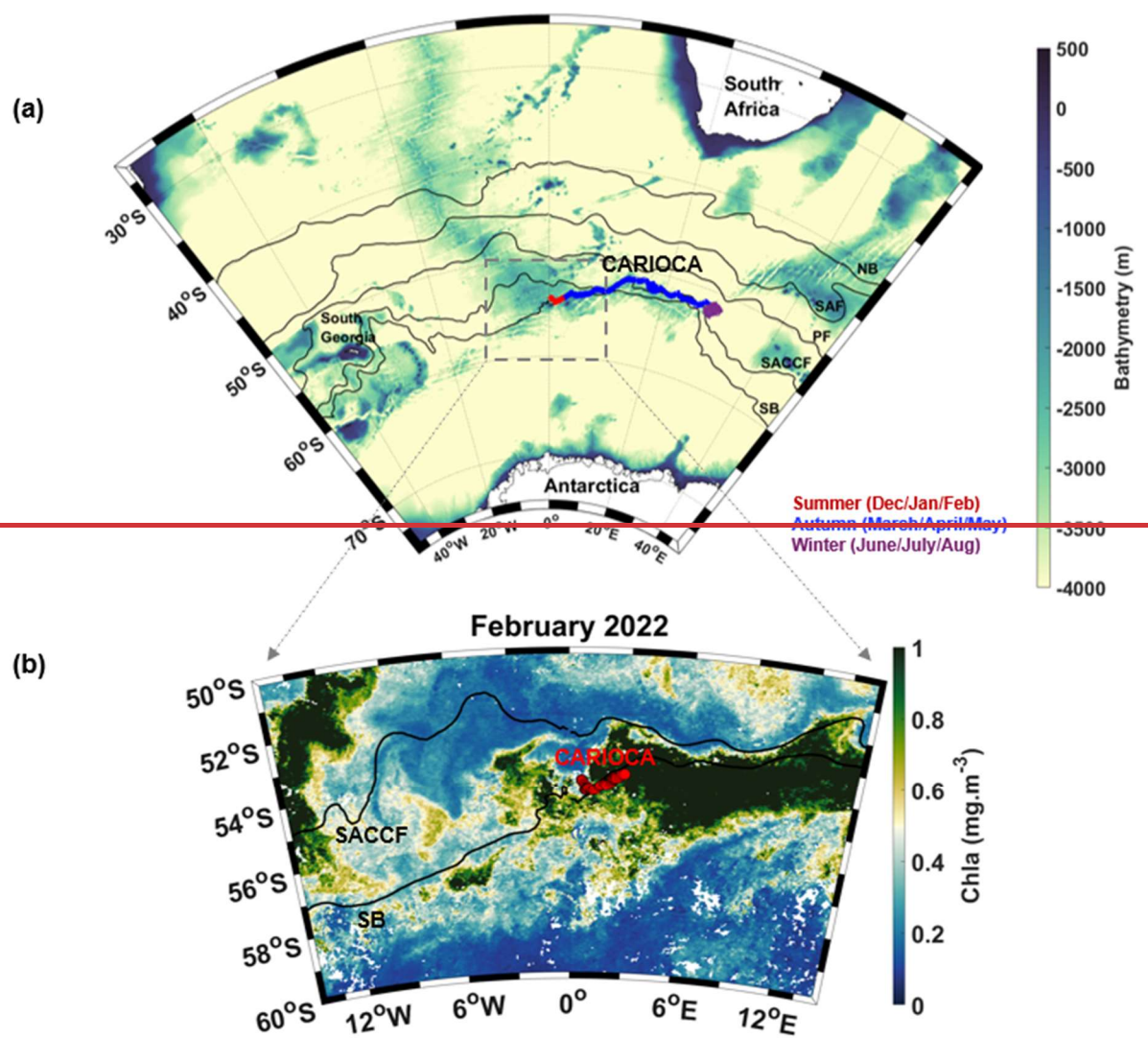
According to the latest Global Carbon Budget, atmospheric CO₂ concentrations keep increasing and are projected to be 51% higher than pre-industrial levels in 2023. The ocean helps mitigate the atmospheric CO₂ increase by acting as a carbon sink. Indeed, during the past decade (2013-2022), the global ocean absorbed $2.9 \pm 0.4 \text{ Gt C yr}^{-1}$, representing 26% of worldwide CO₂ emissions annually (Friedlingstein et al., 2023). The Southern Ocean plays an important role in the ocean's buffering capacity. Defined as the ocean surrounding Antarctica, south of 30°S – 35°S, it covers only about 20-30% of the global ocean surface, yet serves as a main pathway for anthropogenic carbon uptake (Frölicher et al., 2015; Gruber et al., 2019). It is, in fact, responsible for about 40% of the global oceanic uptake of anthropogenic CO₂ (DeVries, 2014; Frölicher et al., 2015; Gruber et al., 2019; Mayot et al., 2023).

The direction of the air-sea CO₂ flux is determined by the difference between the fugacity of CO₂ at the ocean surface, fCO₂, and in the atmosphere, fCO_{2atm}. When the fCO₂ is undersaturated with respect to the atmosphere, the ocean is a carbon sink (Wanninkhof, 2014). Any process that affects fCO₂ at local or regional scale, like the biological activity, or the ocean circulation, can therefore affect the ocean carbon pump (Henley et al., 2020). Ultimately, it is the balance between the biological pump, the solubility pump, and ocean circulation which will determine whether the surface ocean will behave as a sink or a source of carbon to the atmosphere.

The lack of fCO₂ observations have posed a daunting challenge to the ocean community to understand the full suite of mechanisms controlling the air-sea CO₂ flux, and to assess its net magnitude. This is particularly true in the Southern Ocean, which is renowned to be pivotal in controlling global air-sea CO₂ flux, but is also one of the regions suffering the most from fCO₂ observation scarcity. As a result, there are large discrepancies in the Southern Ocean carbon sink estimates from the literature, (sink south of 30°S derived from fCO₂ products: 1.6 [1.3, 1.7] Gt C yr⁻¹, inversion estimates: 1.5 [1.3, 1.9] Gt C yr⁻¹, GOBMs: 1.4 ± 0.3 Gt C yr⁻¹), which result in large uncertainties in our global estimates of air-sea CO₂ flux (Friedlingstein et al., 2023).

The difficulty to assess CO₂ uptake by the Southern Ocean is exacerbated by the fact that this the Southern Ocean carbon sink is much more variable than previously thought. This basin has a large interdecadal variability, and that observation-based products, such as those derived from SOCAT (Bakker et al., 2016), and Global Ocean Biogeochemical Models (GOBMs) have shown different interannual trends for the past years. Present-day fCO₂ products may overestimate the decadal variability of the Southern Ocean carbon sink by 50%–130% due to data sparsity (Hauck et al., 2023). When derived from the fCO₂ product, mean decadal amplitude is 6.31 Tmol yr⁻¹ and mean interannual amplitude is 1.68 Tmol yr⁻¹. On the other hand, when derived from the GOBMs, both mean decadal amplitude and mean interannual amplitude is 2.1 Tmol yr⁻¹ (Mayot et al., 2023). In this regard, a better understanding of the different processes governing the air-sea flux of CO₂ is essential ~~in order~~ to anticipate the effects of climate change on the Southern Ocean's capacity to continue sequestering carbon (Hauck et al., 2023; Mayot et al., 2023; Meijers et al., 2023). Indeed, although the carbon sink significantly strengthened since the early 2000s, a shift in climate trends could cause the Southern Ocean to lose its newly regained capacity for carbon uptake (Landschützer et al., 2015). To better monitor carbon related properties, there has been an increased deployment of BGC-ARGO floats via the SOCCOM project (Sarmiento et al., 2023) and recent studies using uncrewed surface vehicles (Nicholson et al., 2022; Sutton et al., 2021).

70 The SO-CHIC (“Southern Ocean Carbon and Heat Impact on Climate”) European programme was launched to
71 tackle this knowledge gap (The SO-CHIC consortium et al., 2023). In this context, during the *S.A. Agulhas II*
72 summer research cruise in January 2022 (Ward et al., 2022), a CARIOCA (“CARbon Interface Ocean
73 Atmosphere”) buoy was deployed near the Southern Boundary, north-east of the Weddell Sea, and west of Bouvet
74 Island (~~Naëek et al., 2024~~). At the same time, an underwater ocean glider (~~675SG675~~) (~~Swart et al., 2024~~),
75 alongside deep CTD sections (~~Steiger et al., 2022~~) were deployed. The glider followed the buoy for six weeks to
76 provide observations of the underlying ocean conditions. The CARIOCA buoy acquired fCO₂ measurements in
77 the subpolar region (Fig. 1) where surface fCO₂ observations have been sparse in the past twenty years (Gruber et
78 al., 2019).



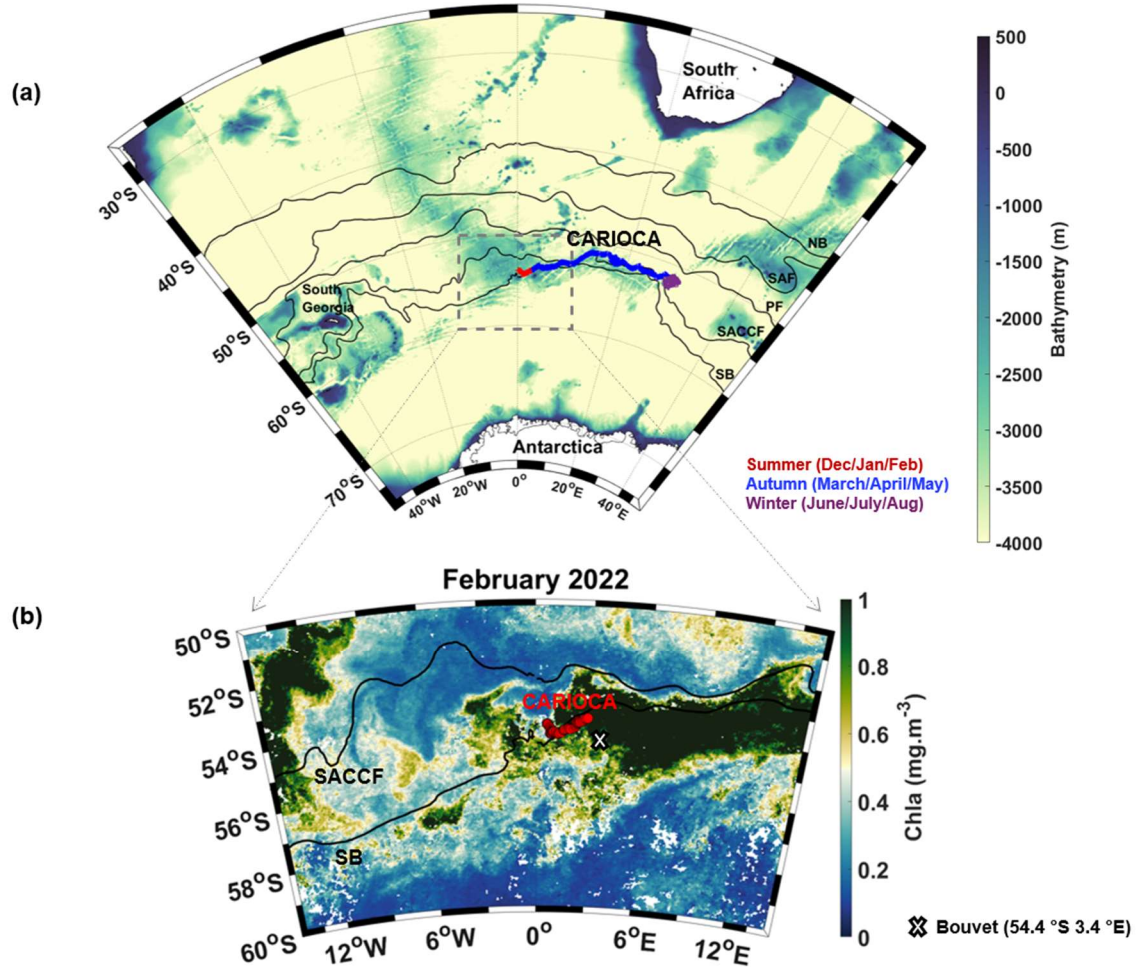


Figure 1: (a) CARIOCA trajectory from 26 January 2022 to 27 June 2022 superimposed on a bathymetry map of the study zone. Fronts from Park & al. 2019 are indicated, from north to south: Northern Boundary (NB) of the ACC, Subantarctic Front (SAF), Polar Front (PF), Southern Antarctic Circumpolar Current Front (SACCF) and Southern Boundary (SB) of the ACC. (b) CCI Chl-a map with CARIOCA trajectory in February.

In this paper, we use these unique field observations to investigate the cause of fCO_2 variations along the trajectory of the buoy, with a particular focus on the role of biological activity in shaping these variations. The Southern Ocean is a High Nutrient Low Chlorophyll (HNLC) region, with iron as the key limiting nutrient for phytoplankton growth. ~~Sources of iron to the ocean mixed layer therefore condition the efficiency of the biological carbon pump. Iron can come from island/plateau sources, ocean ridge sources or from an sea ice source (Ardyna et al., 2019). In summer 2022, west and north-east of Bouvet Island (54.42°S 3.34°E, Fig. 1), an unusually large CO_2 sink was observed along the path of the buoy, as well as high biological activity. This study aims to investigate the processes that contributed to this summer 2022 large CO_2 sink. In the next section the instruments deployed, the different data sets and the methodology used will be described. There will then be a description of the results followed by a discussion.~~ Sources of iron to the ocean mixed layer therefore condition the efficiency of the biological carbon pump (Ardyna et al., 2019; Blain et al., 2008; Boyd, 2007). Iron can come from island/plateau sources, ocean ridge sources, entrained of Fe-rich waters (Tagliabue et al., 2014) or from a sea ice source (Ardyna et al., 2019). In summer 2022, west and north-east of Bouvet Island (54.4°S 3.4°E, Fig. 1), an unusually large CO_2 sink was

observed along the path of the buoy, as well as high biological activity. This study aims to investigate the processes that contributed to this large summer 2022 CO₂ sink.

2. Materials and methods

2.1 CARIOCA measurements

The CARIOCA buoy was deployed on 24²³ January 2022 at 54°S, 0°W. It ~~was anchored at 15 m depth and followed~~has a floating anchor, following the currents at 15 m depth, in a quasi-Lagrangian way. A three-wavelength spectrophotometer (434, 596 and 830 nm) was used to measure fCO₂. The fCO₂ sensor included an exchanger where a dye solution (thymol blue) was brought into equilibrium with seawater via a semi-permeable CO₂ membrane. The absorption coefficient of the dye was measured by the spectrophotometer and was then related to the carbonate properties of seawater. The three-wavelength measurements enable correction of any modification of the optical path or of the opacity of the optical cell (Copin-Montégut et al., 2004). The ~~absolute precision~~accuracy of the fCO₂ is estimated $\pm 3 \mu\text{atm}$ and its ~~relative~~precision is $\pm 1 \mu\text{atm}$. (Boutin et al., 2008). A thermosalinograph measured the sea surface temperature at 2 m depth, SST, and the conductivity, from which sea surface salinity, SSS, was derived. An optode measured dissolved oxygen (O₂). ~~According to the manufacturer, the precision of the O₂ measurements is $\sim 8 \mu\text{mol L}^{-1}$ (5 %).~~ Calibrated values were given by the manufacturer for pure water, and they were corrected from the effects of temperature and salinity as described in Merlivat et al. (2015). A fluorometer measured the fluorescence which was calibrated in Chl-a units using the calibrated Seaglider ~~(675) fluorescence~~SG675) Chl-a (see section 2.3). An anemometer measured wind speed, and a barometer measured atmospheric pressure (Patm) at 2 m above the sea surface. The wind at 10 m above the ocean was derived assuming a neutral atmosphere. As from 4 June 2022, the CARIOCA atmospheric sensor stopped working, and the wind and atmospheric pressure data were replaced with data from ERA5 ~~(C3S, 2018)~~. During their common period, CARIOCA and colocated ERA5 data were very similar (mean difference = 0.26 m s^{-1} , $R^2 = 0.86$, not shown). The CARIOCA measurements, sensors and accuracy are summarized in Table 1. The buoy acquired 17 months of data which was transmitted in real time via ARGOS, and stopped functioning on the 24 June 2023. In this study, we only use observations from ~~the period of~~ 26 January 2022 to 27 June 2022, ~~which corresponds to the time period~~ during which a strong CO₂ sink undersaturation of ocean fCO₂ with respect to the atmosphere was observed in January-March and gradually declined until June.

Table 1: CARIOCA sensors description

<u>Measurement</u>	<u>Type of sensor</u>	<u>Accuracy</u>
<u>fCO₂</u>	<u>CARIOCA Spectrophotometer (manufactured by NKE-France), using a semi-permeable membrane, thymol blue dye and doing measurements at three wavelengths</u>	<u>$\pm 3 \mu\text{atm}$ (Boutin et al. 2008)</u>
<u>SST</u>	<u>Seabird Microcat SBE 37 SI probe</u>	<u>$\pm 0.002 \text{ }^\circ\text{C}$ (-5 to 35 °C)</u>
<u>Conductivity</u>	<u>Seabird Microcat SBE 37 SI probe</u>	<u>$\pm 0.003 \text{ mS cm}^{-1}$</u>
<u>Dissolved oxygen</u>	<u>Optode 4835 (Aanderaa)</u>	<u>$16 \mu\text{mol kg}^{-1}$ (5%)</u>

<u>Chl-a</u>	<u>Seabird WetStar fluorometer</u>	<u>0.1 mg m⁻³ (derived from CTD – glider calibration)</u>
<u>Wind speed</u>	<u>Anemometer</u>	<u>± 3%</u>
<u>Atmospheric pressure</u>	<u>Barometer</u>	<u>± 0.5 hPa</u>

2.2 CARIOCA derived parameters

The air-sea F flux of CO₂ represents the exchanges of CO₂ at the ocean-atmosphere interface. It This air-sea flux of CO₂ (F) was calculated using Wanninkhof's methodology (Wanninkhof, 1992, 2014)-bulk formula as:

$$F = K (f\text{CO}_{2\text{ssw}} - f\text{CO}_{2\text{atm}}) \quad (1)$$

where $f\text{CO}_{2\text{ssw}}$ and $f\text{CO}_{2\text{atm}}$ are the fugacity of CO₂ at the ocean surface and in the atmosphere and K is the CO₂ exchange coefficient (Wanninkhof, 1992, 2014). The $f\text{CO}_{2\text{atm}}$ was determined using atmospheric CO₂ concentration data ($x\text{CO}_2$ atm) from SPO (“South Pole Antarctica”), and CARIOCA Patm according to Eqn. 2 in Boutin et al. (2008).

To eliminate $f\text{CO}_2$ changes linked to temperature and salinity, the concentration of dissolved inorganic carbon (DIC) was estimated. At given SST and SSS, the DIC and alkalinity ~~waswere~~ estimated from $f\text{CO}_2$. The alkalinity was calculated according to Lee et al. (2006). The Matlab routine *CO2SYS*, with dissociation constants K1 and K2 of Lueker et al. (2000) was used to derive DIC. Oxygen saturation ($\text{O}_{2\text{sat}}$), the degree of oxygen saturation ($\text{pO}_{2\text{sat}}$) and the oxygen flux at the air-sea interface (FO_2) were calculated as per Merlivat et al. (2015). The oxygen anomaly was calculated by subtracting the dissolved oxygen concentration calculated at saturation from the dissolved oxygen concentration ($\text{O}_2 - \text{O}_{2\text{sat}}$). During photosynthesis, a positive anomaly is expected whereas during respiration / remineralization, a negative anomaly is expected. The oxygen measurements of the CARIOCA drifter could not be recalibrated at sea, because unfortunately the O_2 measured by the CTD at the deployment was not calibrated. An empirical correction of $+8 \mu\text{mol} \cdot \text{kg}^{-1}$ ~~(which corresponds to the precision of the optode)~~⁻¹ was applied to bring the values of $\text{O}_2 - \text{O}_{2\text{sat}}$ above zero, during periods of high biological activity. These high biological periods are detected from CARIOCA fluorescence and opposite variations in O_2 and DIC. The carbon net community production, NCPc , and the oxygen net community production, NCPo_2 , were estimated during periods of high biological activity, during which diurnal cycles with DIC and $\text{O}_2 - \text{O}_{2\text{sat}}$ in opposition were observed by the CARIOCA buoy, ~~following the same methodology as in Merlivat et al. (2015), using mixed layer depth (MLD) derived from glider vertical profiles. FO_2 was used when estimating NCPo_2 , following the same methodology as in Merlivat et al. (2015), but using the mixing layer depth as in Merlivat et al. (2022) and Pellichero et al. (2020)~~ (see section 2.3).

2.3 Seaglider measurements and derived parameters

~~The Seaglider (SG675)~~ A Kongsberg Seaglider (SG675) was deployed alongside the CARIOCA buoy. A Seaglider is an autonomous underwater vehicle designed to fly through the water column from the sea surface to 1000 m depth following a sawtooth pattern, moving vertically and horizontally at nominal speeds of 0.1 m s⁻¹ and 0.3 m s⁻¹, respectively. Upon surfacing roughly every 6 hours, Seagliders communicate to base station via Iridium, thereby transferring data in near-real time. A key characteristic of Seagliders is their ability to be piloted from land, allowing researchers to control the direction of sampling. For this experiment, SG675 followed the CARIOCA buoy for a month and a half, from 31 January 2022 to 10 March 2022 (39 days) (Fig. 1), providing vertical profiles

of temperature, salinity, oxygen and fluorescence of the upper 1000 m of the water column. There was a time lapse of about one day between CARIOCA and the glider, the glider being about one day behind the buoy each time. ~~Both instruments were less than 20 km apart during that period.~~ For this study, only profiles between the 31 January and the 10 March 2022 were considered, which was when the glider and the CARIOCA were nearest to each other. ~~(less than 20 km apart).~~ The glider data was processed using the “GliderTools” package (Gregor et al., 2019; ~~Swart et al., 2024~~). For the salinity data, outliers and spikes were removed and a smoothing was applied with Savitzky-Golay filter. The glider salinity data was also validated using the CTD salinity profile ~~at the time of deployment~~ (on the 23 January 2022 14h46). The CTD salinity data had already been calibrated, and the CARIOCA SSS data was in turn validated using the already validated glider surface salinity data. The glider salinity at 2 m and the CARIOCA SSS (at 2 m), were in good agreement, with a small difference of about 0.05 pss. Using “GliderTools” ~~”~~ ~~(Gregor et al., 2019)~~, the glider fluorescence profiles were also quality controlled. Outliers, spikes and bad profiles were removed, and the data was corrected for in situ dark counts. A quenching correction using the same method as Thomalla et al., 2018 was applied. The glider fluorescence was calibrated and converted to chlorophyll-a using the ~~CTD fluorescence at the time of chlorophyll-a CTD water samples, less than 24 h after~~ deployment. The mixed layer depth, MLD, was estimated ~~using from~~ the glider data using the density threshold of 0.03 kg m^{-3} (de Boyer Montégut et al., 2004) ~~”~~. It has been observed in past studies that DIC can be more sensitive to the mixing layer, XLD, which can be determined using turbulence measurements (Nicholson et al., 2022; Pellichero et al., 2020; Sutherland et al. 2014; Giunta and Ward 2022). The empiric relationship approximated by Nicholson et al. (2022) was used to estimate XLD. (The MLD and the XLD are surface layers directly influenced by the atmosphere. The MLD has homogenised, formed as a result of mixing, while the XLD is still actively influenced by turbulence and still mixing).

2.4 *S.A Agulhas II* TSG

The *S.A. Agulhas II* was equipped with a thermosalinograph (TSG) ~~(Ward et al., 2024)~~, and ship measurements of salinity and temperature were collected, from South Africa to Antarctica, and back again, from the 3 December 2021 to the 28 January 2022. The *S.A. Agulhas II* TSG SSS data was calibrated using underway water samples collected during the SO-CHIC cruise (Ward et al., 2022).

2.5 Satellite, analysis, and reanalysis datasets

Chlorophyll-a satellite images are from the Climate Change Initiative product version 6.0 (OceanColour - CCI, 2024), from 1997 to 2022, for spring (November: 1997-2021) and summer (January, February: 1998-2022). Monthly and weekly means were used for the Chl-a. For the surface salinity data, Glorys reanalysis (Global Ocean Physics Reanalysis, 2024), Mercator analysis (Global Ocean Physics Analysis and Forecast, 2024) at 5 m depth, SMOS CATDS CECv9.0 (18 days) satellite data (Boutin et al., 2023) ~~and ISAS analysis at 5 m depth (In Situ Analysis System, an optimal interpolation from ARGO floats) (Szekely et al., 2024) were used. A colocalization between Mercator / Glorys salinity data and CARIOCA SSS indicates that both datasets were in good agreement, showing similar patterns, but with Mercator / Glorys salinity data being lower than the CARIOCA by about 0.1 pss from February 2022 to mid April 2022 (Fig. B1 in Appendix).~~

were used. Daily and monthly data, from Mercator analysis were used as of July 2021, and Glorys reanalysis was used for the years before July 2021. A colocalization between Mercator salinity data and CARIOCA SSS indicates that both datasets were in good agreement, showing similar patterns, but with Mercator salinity data being lower than the CARIOCA by about 0.1 pss from February 2022 to mid-April 2022 (Fig. A1 in Appendix).

The Mercator/Glorys products were also used to analyse vertical salinity (not shown) and surface current velocities. Sea ice data was obtained from OSI SAF (EUMETSAT - Product Navigator - Global Sea Ice Concentration Climate Data Record v3.0 - Multimission, 2024; EUMETSAT - Product Navigator - Global Sea Ice Concentration Interim Climate Data Record Release 3 - DMSP, 2024).

2.6 Lagrangian analysis

Backward trajectories of water masses were computed with a Lagrangian analysis (Sergi et al., 2020) using the LAMTA software (Rousselet, L et al., 2024 pre-print). After initialising the particles at specific dates, longitudes and latitudes, a backward advection was performed to estimate the trajectories of these particles several months before. To determine which water masses reached the CARIOCA, particles were initialised at the CARIOCA coordinates, with one coordinate point per hour (i.e. 24 points advected backwards in time each day). Three current products were tested, namely, GlobCurrent (Global Total (COPERNICUS-GLOBCURRENT), Ekman and Geostrophic currents at the Surface, 2024), Mercator Analysis (Global Ocean Physics Analysis and Forecast, 2024) / Glorys reanalysis (Global Ocean Physics Reanalysis, 2024) and OSCAR (OSCAR third degree resolution ocean surface currents | PO.DAAC / JPL / NASA, 2024)- (Fig. S1 in Supplement). Using Mercator analysis / Glorys reanalysis, different depths were also tested, namely 5 m, 15 m, 34 m and 55 m. Using OSCAR, the backward trajectories in November, January and February were also computed, from 1997 to 2022. In the next sections, we are showing the results obtained using the total currents, i.e. the sum of the geostrophic and Ekman currents, at 15 m depth. The reliability of numerical trajectories for reconstructing phytoplanktonic blooms from nutrient sources and up to mesoscale precision has been validated in the Southern Ocean from multi satellite data, surface drifters, and lithogenic isotopes (Sergi et al. 2020; d'Ovidio et al. 2015; Sanial et al. 2014).

3. Results

3.1 CARIOCA and Seaglider observations



Figure 2: CARIOCA time series from the 26 January 2022 to the 27 June 2022: (a) Atmospheric and surface ocean fCO₂ (fCO_{2atm} and fCO₂), and daily mean of CO₂ flux, (b) DIC and wind speed, (c) SST and SSS, (d) Chl-a and O₂-O₂sat, with the period during which the glider followed the buoy (31 January to 10 March 2022) indicated by dotted lines. The thinner dotted lines show the data derived from ERA5 (fCO₂ atm and CO₂ flux derived from ERA5 Patm, and ERA5 wind, as from the 4 June 2022). The whole time series from the 26 January 2022 to the 24 June 2023 is shown on Fig. S2 of the Supplement.

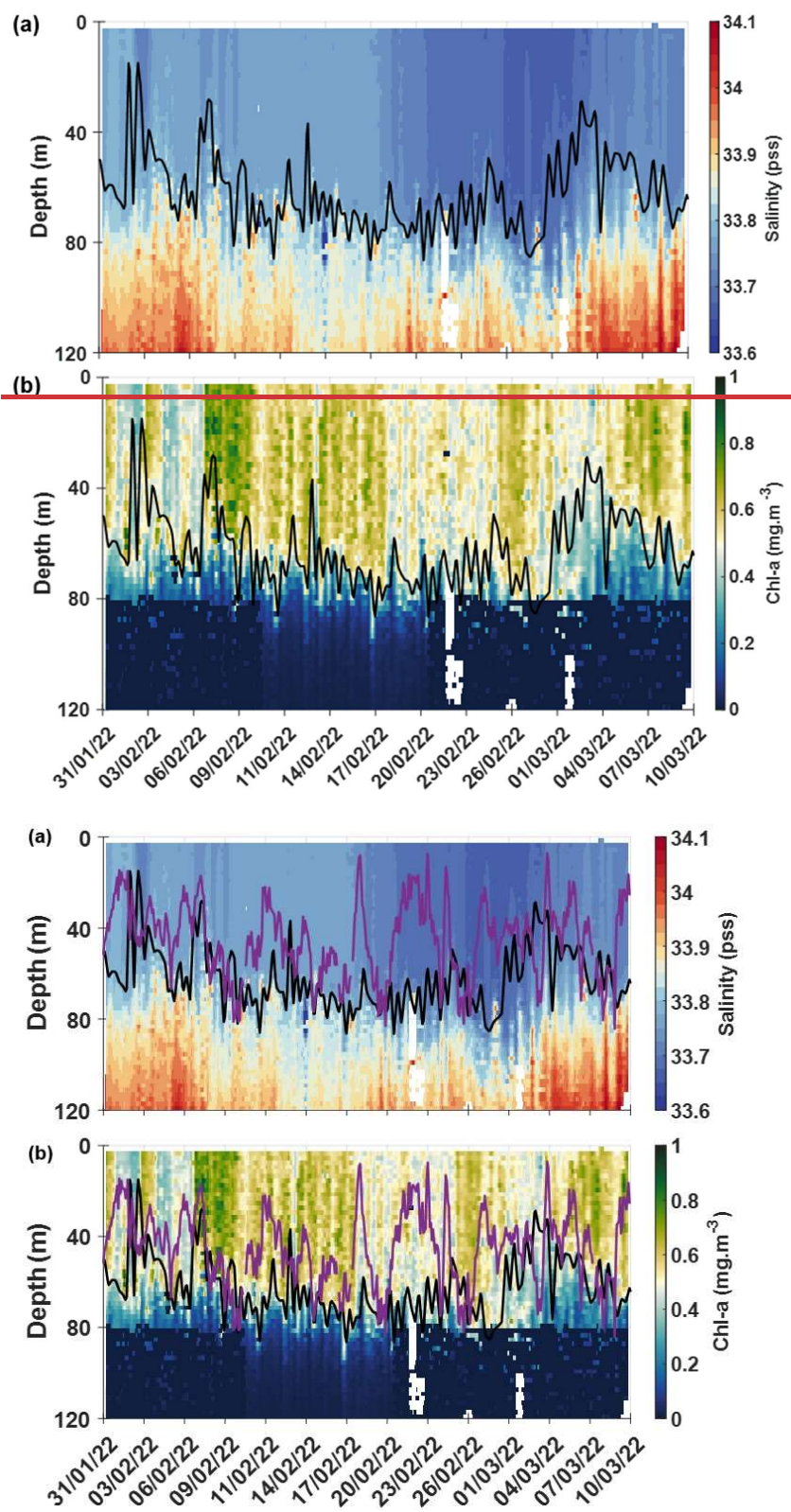


Figure 3: Seaglider profile time series between the 31 January and the 10 March 2022 of (a) salinity, (b) Chl-a, with the MLD indicated with the (black line) and the XLD (purple line).

Low surface salinities were measured in February 2022, both by the CARIOCA buoy (Fig. 2 (c)) and by the glider (Fig. 3 (a)) with minimum values of salinity in the second half of February. The CARIOCA measured surface

salinities around 33.7 pss between 17 February and 8 March 2022. Both the glider and the CARIOCA observed maximas of surface Chl-a around the 7 February and the 7 March 2022 (Fig. 2 (d) and Fig. 3 (b)). According to the glider profiles, the low values of salinity, and high concentrations of Chl-a, observed from early February to early March, were well mixed within the mixed-layer, confined to the top 60 m or so (Fig. 3). According to fig. 2 (a), a very low $f\text{CO}_2$ was observed by the CARIOCA in summer 2022, while the buoy was in this fresh water mass, enriched in Chl-a and oxygen. The $\text{d}f\text{CO}_2$ is about $-60 \mu\text{atm}$ from the end of January to the end of March 2022. Minima of $f\text{CO}_2$ ($\sim 320 \mu\text{atm}$) and of DIC ($\sim 2120 \mu\text{mol kg}^{-1}$) occurred on the 7 February and the 7 March 2022, which also coincided with maximum concentrations of chlorophyll-a ($\sim 1.3 \text{ mg m}^{-3}$) and of oxygen. Around these dates, diurnal cycles of DIC and $\text{O}_2\text{-O}_{2\text{sat}}$, with the DIC and $\text{O}_2\text{-O}_{2\text{sat}}$ in opposite phases were clearly observed, and allowed NCP estimates (see next section). According to CARIOCA measurements (Fig. 2 (a)), after March, as the CARIOCA drifted away from the phytoplankton bloom, $f\text{CO}_2$ started increasing, until it reached values close to equilibrium with the atmosphere on 27 June 2022. The CARIOCA derived air-sea CO_2 flux averaged to $-18.8 \text{ mmol m}^{-2} \text{ day}^{-1}$ from January to March 2022, and after March it started increasing until it reached values close to zero in June 2022.

3.2 NCP and impact of wind on MLD XLD

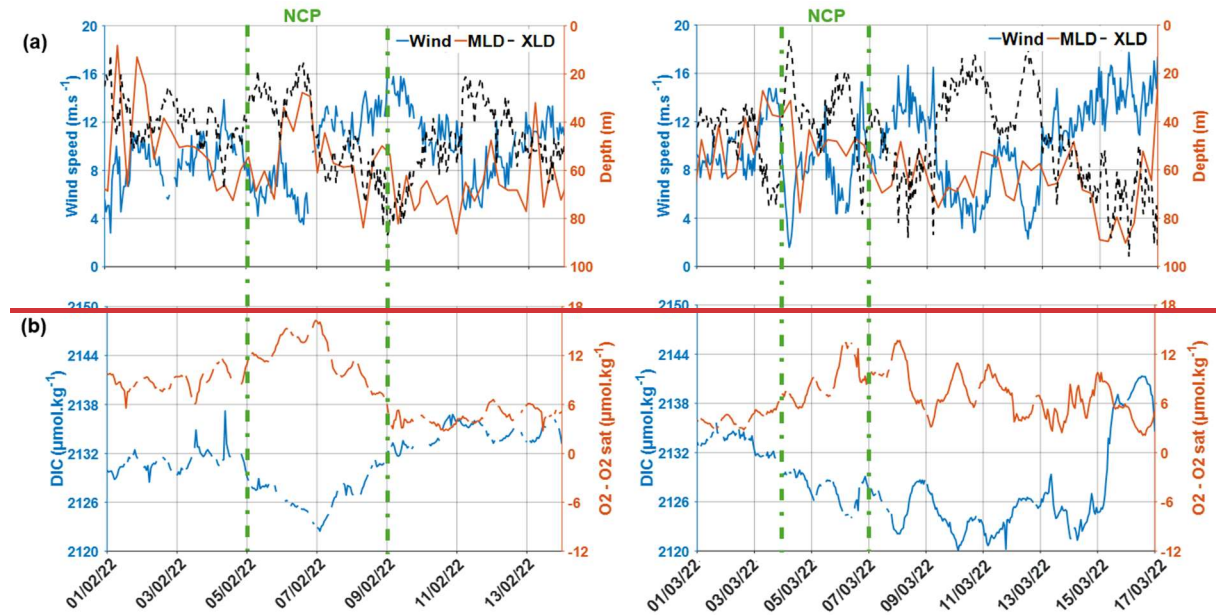


Figure 4: CARIOCA time series, during NCP periods on the 5-9 February 2022 (left), and on the 4-7 March 2022 (right), (a) Wind speed, MLD and (b) DIC and $\text{O}_2\text{-O}_{2\text{sat}}$.

During the two periods dominated by biological activity, on the 5-9 February 2022, and on the 4-7 March 2022, Chl-a increased by 0.5 mg m^{-3} and DIC decreased by $10 \mu\text{mol kg}^{-1}$ (Fig. 2, Fig. 4 and Fig. A1B1 in Appendix AB). Just before the peaks of Chl-a (corresponding to minimum concentrations of DIC and maximum concentrations of oxygen), there were very low wind speeds, associated with a shoaling of the mixed layer and mixing layers (Fig. 2 and Fig. 4B1), which itself might have enhanced Chl-a bloom at the surface (Fig. 3- (b)). During the February event, NCPc was estimated to reach $-91 \text{ mmol m}^{-2} \text{ d}^{-1}$, while NCPo_2 was $132 \text{ mmol m}^{-2} \text{ d}^{-1}$. During the March event, NCPc of $-104 \text{ mmol m}^{-2} \text{ d}^{-1}$ and NCPo_2 of $138 \text{ mmol m}^{-2} \text{ d}^{-1}$ were estimated (Fig. A1B1 in Appendix). It is

interesting to note that the two values of the photosynthetic quotient, $PQ = NCP_{O_2} / NCP_C$, respectively equal to 1.45 and 1.33 are in close good agreement with the value 1.4 expected in a new production regime (Laws, 1991).

After the 7 February and the 15 March 2022, there was a strengthening of wind speeds, and a deepening of the XLD became deeper than the MLD, probably entraining waters rich in DIC from the subsurface layer. Indeed, the CARIOCA ~~measured derived DIC were~~ higher ~~concentrations of DIC~~ at the same time as higher wind speeds, and lower concentrations of $O_2 - O_{2sat}$ and of Chl-a (Fig. ~~2 and Fig. 4~~) 2 and Fig. B1). The DIC and O_2 changes derived from the CARIOCA measurements are also consistent with the orders of magnitude that could be estimated, using GLODAP climatological DIC and O_2 profiles (not shown), considering the change in XLD. This might suggest that mixing events driven by high winds sometimes compensated for the CO_2 undersaturation driven by biological activity.

However, the mixing events shown here are only on synoptic time scales. For instance, after the 10 February 2022, the wind decreased again and DIC concentrations stopped increasing (Fig. ~~4 (a)~~). ~~Overall, the CARIOCA measured low fCO_2 and DIC concentrations coinciding with high concentrations of Chl-a and oxygen, during the whole summer 2022. This suggests that biological activity was the dominant driver of the DIC seasonal variation, but the overall DIC concentration might have been even lower without wind-driven mixing. B1 (a)). In fact, outside the brief periods of local biological production and of mixing events, the DIC and the fCO_2 remained relatively stable at a low value from January to March. For instance, between the 11/02/2022 and the 03/03/2022, the DIC remained at a mean value of $2133 \mu mol kg^{-1}$ (Fig. 2).~~

3.3 Origin of fresh water mass and phytoplankton bloom

In summer 2022, the CARIOCA and glider were found in productive waters of low salinity (Fig. 2 and 3). The presence of this low salinity upper ocean was also confirmed by the *S.A Agulhas II* thermosalinograph SSS observations. Moreover, SSS images from the SMOS satellite mission, as well as salinity estimates, at 5 m, from an ocean analysis (Mercator) ~~and reanalysis (Glorys), and from an observational based gridded ocean salinity estimate (ISAS), are all~~, are in agreement with the in-situ measurements and show low salinities in that region, in summer 2022 (Fig. ~~B2C1~~ in Appendix ~~BC~~). This surface fresh layer suggests a stratification of water masses, which might have favoured the sustained growth of phytoplankton in a shallow mixed layer, where more light was available.

To investigate the origin of these waters, we computed backward trajectories of virtual particles that were released at the CARIOCA location. These particles were advected backward in a suite of different velocity field estimates, ~~at 15 m depth~~ (see Methods). According to salinity maps from Mercator/~~Glorys, (not shown)~~, and to backward trajectories spanning several months before the 2022 deployment of the instruments, the fresh water mass in which the CARIOCA and glider drifted was advected from a region south-west of their position, close to the sea ice edge, in the Weddell Sea. ~~The formation of this fresh water mass can be seen, from September to December 2021, using salinity maps and sea ice data from OSI SAF (Fig. C1 in Appendix). The decrease in salinity started near the South Sandwich trench, around $25^\circ W$ and $60^\circ S$, near the sea ice edge in September 2021, when the sea ice started to retreat. It continued to develop eastward near the sea ice edge until November 2021 (Fig. C1 in Appendix). Fig. 5 (b) shows the sea ice retreat that month and the decrease in salinity that is very likely due to ice melt. The water mass then travelled north-east (Fig. C1 and Fig. E1 in Appendix). In March 2022, the waters reaching CARIOCA~~

still originated from the south-west but then passed near Bouvet Island, before reaching the CARIOCA (Fig. E1 in Appendix). This corresponds to a decrease in fCO_2 , DIC and increase in Chl-a (Fig. 2).4).

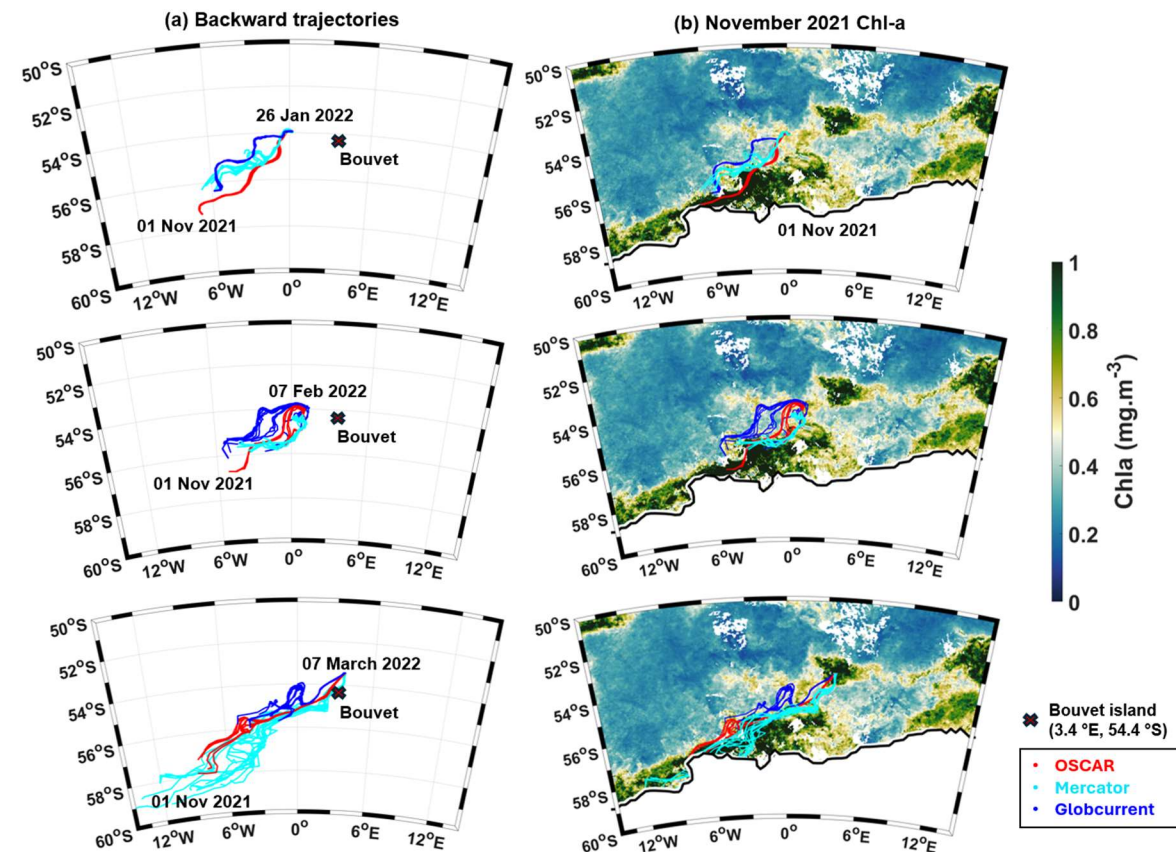
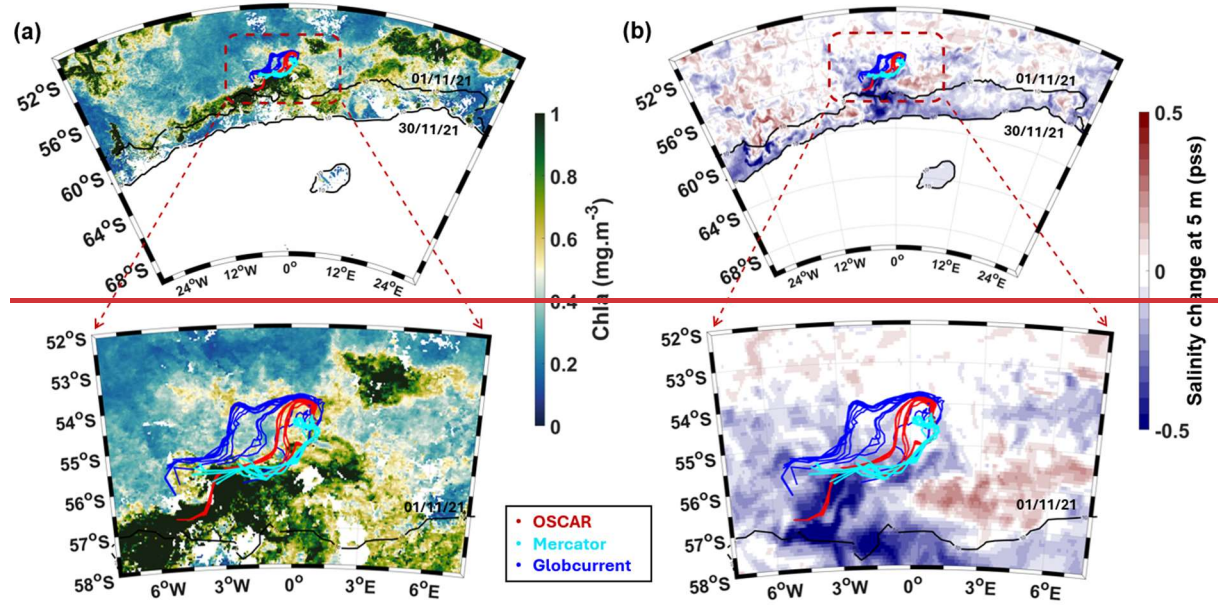


Figure 54: (a) Backward trajectories from CARIOCA's location in January (top), February (middle), and March (bottom) 2022 to November 2021, using different current products (Mercator analysis, OSCAR, Globcurrent). (b) CCI Chl-a in November 2021, with sea ice mask (b) Mercator salinity change at 5 m in November 2021 (difference between the 30 November and 1 November), with black-lines representing the sea ice concentration at 10%, on the 1 November 2021, and on the 30-November 2021. Bottom-figures represent a zoom of the region, with backward trajectories (using

~~Mercator, OSCAR and GlobCurrent total currents at 15 m depth) from the 7 February 2022 (from CARIOCA's location) to the 1 November 2021, superimposed.~~

On Fig. 5, ~~backward trajectories, computed using currents from OSCAR, Mercator / Glorys and GlobCurrent, show that waters found at CARIOCA location (0.8° E, 54° S) on the 7 February 2022, came from a large phytoplankton bloom (high Chl a) that occurred in a region where surface salinity decreased at around 4-5 °W and 55.5-56.5 °S, near the sea ice edge, on the 1 November 2021. This corresponds to an export of waters from the Weddell Sea, south of 55° S (Vernet et al., 2019). No satellite Chl a data is available in October 2021 due to clouds; however we can suppose that there was less sunlight available in October and that the phytoplankton bloom formed in November 2021.~~ 4, backward trajectories, computed using currents from OSCAR, Mercator and GlobCurrent, show that waters found at CARIOCA location on the 26 January 2022 (0.2 °E, 54 °S) and on the 7 February 2022 (0.8° E, 54° S), came from a region around 4-6 °W and 55.5-57°S, near the sea ice edge on the 1 November 2021, where surface salinity decreased and a large phytoplankton bloom (high Chl-a) occurred. The waters reaching the CARIOCA on the 7 March 2022 (3.7 °E, 53.4 °S) originated from a region even closer to the sea ice edge, at around 5-12 °W and 56-59 °S, on the 1 November 2021, and then passed near Bouvet Island, before reaching the buoy. These correspond to an export of waters from the Weddell Sea, south of 55° S (Vernet et al., 2019), which are possibly enriched in dissolved iron originating from sea ice melt (Lannuzel et al., 2016; Person et al., 2021).

3.4 Comparison between ~~spring-summer 2021-2022~~ and ~~2018-2019~~ previous campaigns in summer

~~were conducted at the same season, near 54°S-0°W, in 2019 (Nicholson et al., 2022; Ogundare et al., 2021). A comparison was therefore made between the summers 2022 and 2019. On 19 December 2018, a Wave Glider (a surface autonomous vehicle) was deployed, at 0° E, 54° S (Nicholson et al., 2022). It stayed fixed at this position for about two months, and performed surface measurements, until 11 February 2019. A comparison was made between this Wave Glider and the CARIOCA surface data. The CARIOCA stayed near 0° E, 54° S, from 26 January to 1 February 2022.~~

~~In 2019, the $f\text{CO}_2$ measured by the Wave Glider was near equilibrium with the atmosphere (2019 Wave Glider $f\text{CO}_2 = 410 \mu\text{atm}$) whereas the CARIOCA buoy measured a large CO_2 undersaturation (2022 CARIOCA $f\text{CO}_2 = 330 \mu\text{atm}$, Fig. 2a). In summer 2022 (from 26 January to 11 February 2022) the MLD was around 60 m, whereas in summer 2019 (from 19 December 2018 to 11 February 2019) the MLD was deeper, around 100 m (not shown). According to Nicholson's study, in 2019 the DIC concentration was around $2180 \mu\text{mol kg}^{-1}$, while in January to March 2022 it was much lower ($\sim 2130 \mu\text{mol kg}^{-1}$). After March, as the buoy went out of the Chl a rich waters, the CARIOCA DIC increased gradually, until it reached concentrations around $2170 \mu\text{mol kg}^{-1}$ in June 2022 (Fig. 2 (b)), close to the ones measured by the Wave Glider in 2019.~~

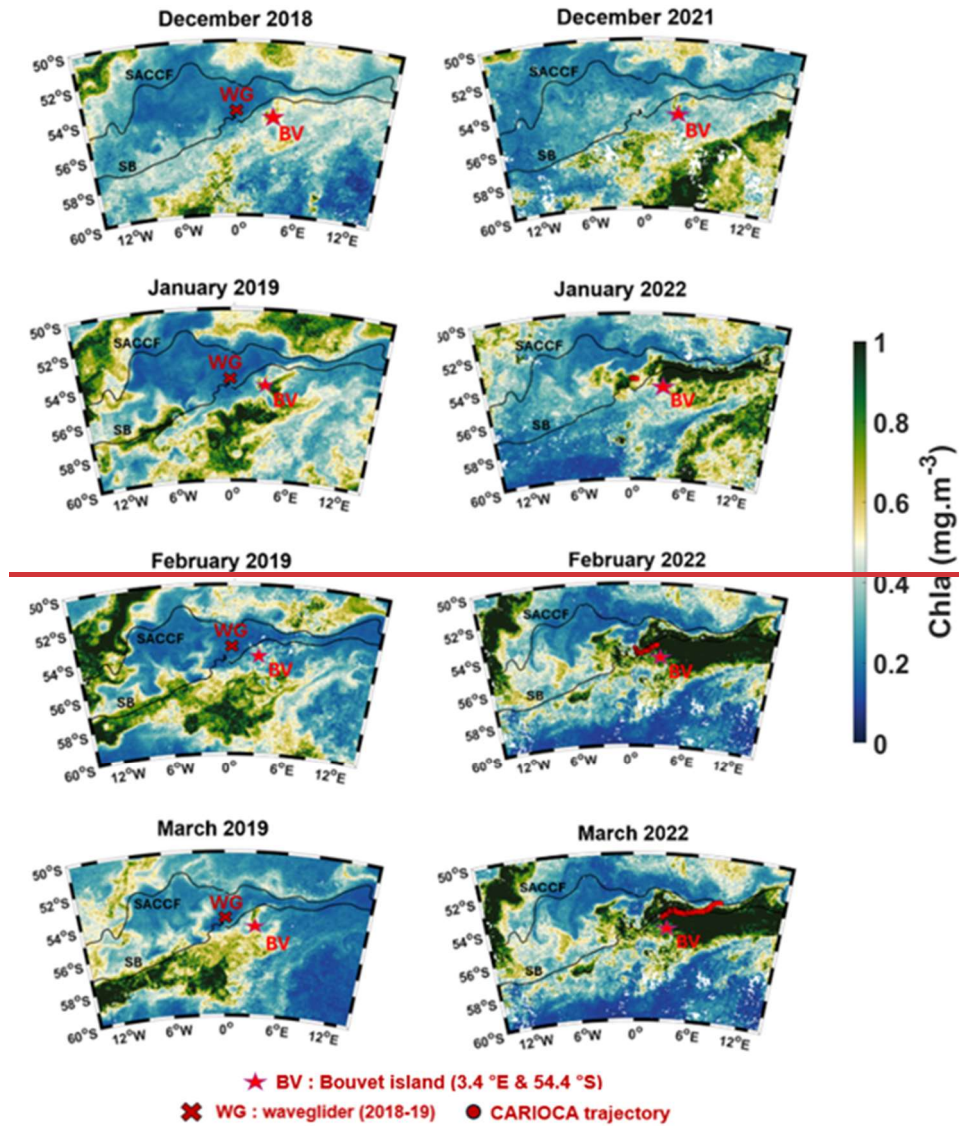


Figure 6: CCI Chl-a maps from December to March, left panel: 2018-2019, with waveglider position for the given month in red, right panel: same as left, but for 2021-2022, with CARIOCA position for the given month in red. (SB: Southern Boundary, SACCF: Southern Antarctic Circumpolar Current Front).

For the Chl-a comparison, CCI data were used to determine the Chl-a concentrations in the region in summer 2019 and 2022 (Fig. 6). From January to March 2022, a large phytoplankton bloom was observed around the Southern Boundary, near the CARIOCA position (Fig. 6 (b)). This phytoplankton bloom was not present at the Wave Glider and CARIOCA locations, in summer 2019 (Fig. 6 (a)). Indeed, around 0° E, 54° S, in 2019, there was no chlorophyll a. So, for different years, at the same position and for the same period, both instruments sampled similar water masses but there was a large CO₂ undersaturation in summer 2022 not present in 2019. This is then likely to be related to the large phytoplankton bloom present, at CARIOCA location, in January 2022. The phytoplankton was farther south in January-March 2019. Indeed, in 2019, the phytoplankton stayed south of the Southern Boundary (SB). The Chl-a concentrations were also lower in summer 2019 compared to 2022, and reached up to 1.5 mg m⁻³ in 2022, whereas in 2019, the maximum Chl-a concentrations did not exceed 1 mg m⁻³. In contrast, in January 2022, the CARIOCA entered in a phytoplankton bloom at 0° E, 54° S. The buoy then continued to sample waters rich in Chl-a in February and March 2022.

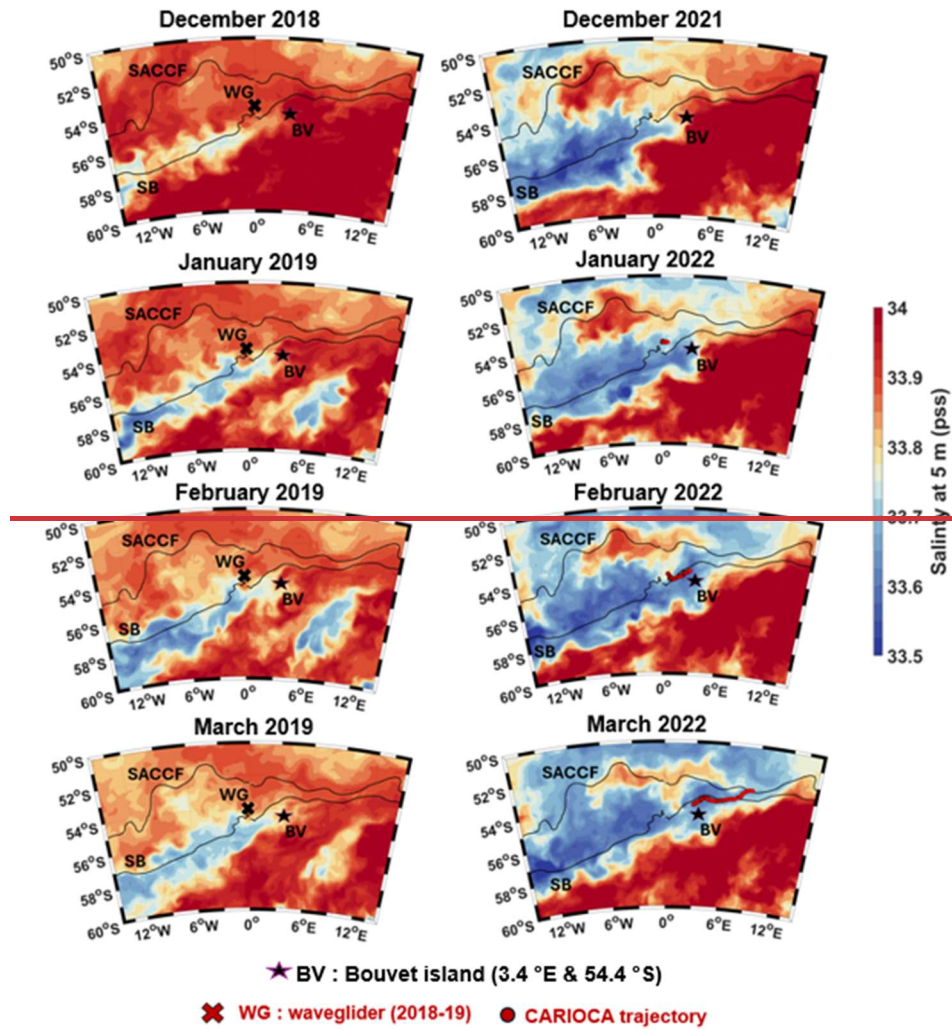


Figure 7: Mercator / Glorys salinity at 5 m, from December to March, left panel: 2018-2019, with waveglider position for the given month in red, right panel: 2021-2022, with CARIOCA position for the given month in red. (SB: Southern Boundary, SACCF: Subantarctic Circumpolar Current Front).

The phytoplankton bloom in summer 2022 in fact coincides with the presence of a fresh water mass. Mercator salinity profiles for spring 2021-summer 2022, show that this lower salinity was only present in the first 60 m, which also corresponds to the glider salinity profile. According to Mercator, in 2019, the lower salinities were much farther south (Fig. 7).

A comparison was also performed with surface transects of the Norwegian RV *Kronprins Haakon* cruise from the 28 February 2019 to the 10 April 2019, (Ogundare et al., 2021). A ship transect crossed the CARIOCA path at around the same dates (end of March/beginning of April for both), for different years (2019 and 2022). North of the Southern Antarctic Circumpolar Current Front (SACCF), in April, the DIC, SST and SSS values for both years were consistent with each other. South of the SACCF, in 2019 the DIC concentration was higher ($\sim 2150 \mu\text{mol kg}^{-1}$) compared to the CARIOCA DIC concentration in 2022 (as low as $2120 \mu\text{mol kg}^{-1}$, South of the SACCF). The ship's path in 2019, south of the SACCF, was between $5-8^\circ \text{E}$ and $53-57^\circ \text{S}$, where the Chl *a* concentrations were low (Fig. 6). At these positions, higher salinities and temperatures were also measured by the RV *Kronprins Haakon*, in 2019 (SSS ~ 34 pss before April 2019) (Fig. D1 in Appendix).

We compare dfCO_2 observed during previous campaigns, using SOCAT and another available dataset (Nicholson et al., 2022) from 2000 to 2022, for the same region and season as in our case study (Fig. 5).

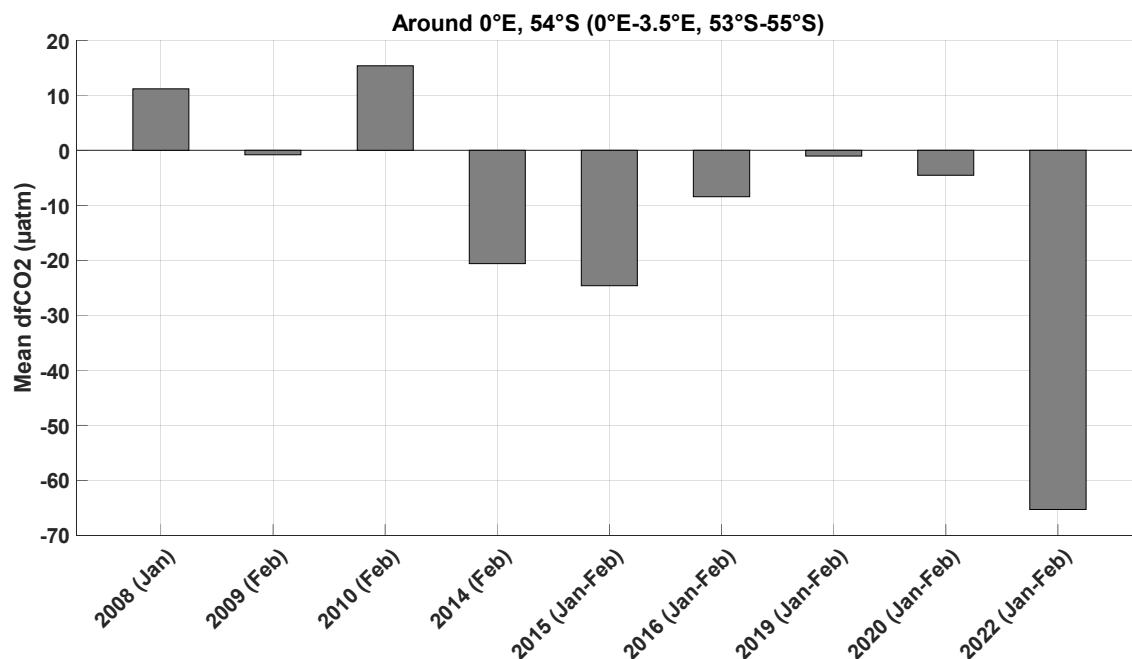


Figure 5: Histogram of dfCO_2 in January and February, estimated using all SOCAT data available between $0^\circ\text{E} - 3.5^\circ\text{E}$ and $53^\circ\text{S} - 55^\circ\text{S}$, from 2000 to 2022. The summer 2019 data is from a Wave Glider (Nicholson et al., 2022).

There was a mean outgassing in summers 2008 and 2010. These years, there was no local bloom observed on CCI Chl-a maps, and we checked with backward trajectories that the waters reaching 0°E , 54°S , did not come from a spring bloom near the ice edge either. On the other hand, in 2014, 2015, 2016 and 2020, an undersaturation smaller than the 2022 one was observed in summer (Jan - Feb) even though there was no local bloom. The waters reaching the region these years, as identified from backward trajectories, came mostly from a bloom near sea ice edge in November (except in February 2014, when the waters came from a bloom occurring in December; in 2016 we could not check due to missing CCI Chl-a data). In 2009 and 2019 the ocean fCO_2 was close to equilibrium with the atmosphere and there was no local bloom. In November 2008, a bloom occurred near the ice edge. However, backward trajectory analysis indicates that the waters reaching the region in February 2009 did not originate directly from the bloom but instead came from areas with lower Chl-a concentrations. The situation in 2019 was comparable. Although there was no bloom in November (2018), a bloom occurred in December (Fig. D1) near the ice edge. However, in the following months, these waters were not advected far enough north and did not reach 0°E , 54°S . Summer 2022 was the summer with the largest negative dfCO_2 around 0°E , 54°S .

The comparison was deepened in summer 2019 (Cf. Appendix D), as this was the year in which the most data from a Wave Glider (Nicholson et al., 2022) and from a ship campaign (Norwegian RV *Kronprins Haakon* cruise) (Ogundare et al., 2021) were available at the same position and same dates as our case study. It showed that in summer 2022, the fresh water mass and phytoplankton bloom were farther north than in summer 2019 (Fig. D1 and D2).

4. Discussion

In summer 2022, the CARIOCA buoy ~~crossed a massive phytoplankton bloom (Figure 1) and~~ measured an unusually large ~~CO₂-sink fCO₂ undersaturation~~ near the Southern Boundary and Bouvet Island, east of 0° E, 54° S (Figure 2a). ~~According to pCO₂. The CARIOCA CO₂ flux integrated over the studied period (26/01/2022 – 27/06/2022) is -1.88 mol m⁻², which, assuming negligible flux the rest of the year, is considerably greater than the climatological values in that region. Actually, according to Gruber et al., 2019 (their fig. 2 (b) - (d)), climatologies (Takahashi et al., 2012) or recent in situ measurements in 2019 (Nicholson et al., 2022; Ogundare et al., 2021), this region is usually in equilibrium with the atmosphere or is a much smaller carbon sink than the one observed in summer 2022.~~ of yearly air-sea CO₂ fluxes are close to 0 mol C m⁻² in the region sampled by the CARIOCA. A comparison to measurements conducted on other summers indicates that summer 2022 was the most undersaturated since 2008 around 0 °E, 54 °S (Cf. Section 3.4). At that time, the CARIOCA crossed a large phytoplankton bloom (Chl-a > 1 mg m⁻³) (Fig. 1b). Sergi et al. (2020) showed that moderate bloom can develop around Bouvet Island by a combination of fertilization from the island itself and from the proximity of seamounts acting as hydrothermal sources of iron. However, the bloom observed in summer 2022 (Fig. 1b) ~~was more massive. In fact, it~~ was the largest bloom observed over the past twelve years (Fig. 8a6) (and ~~also~~ over the last 25 years, not shown), as large as those typically observed on the Kerguelen Plateau (Blain et al., 2007). ~~Moreover, fCO₂ and DIC remain rather stable between January and March, and local biological carbon production appeared to be compensated by entrainment of high DIC into the mixed layer during synoptic mixing events (Nicholson et al., 2022). We thus hypothesize that another process was at play. Indeed, the Lagrangian backward trajectories from the January-February 2022 CARIOCA location are not consistent with an origin from Bouvet Island or from seamounts, in contrast with the case in Sergi et al. (2020).~~

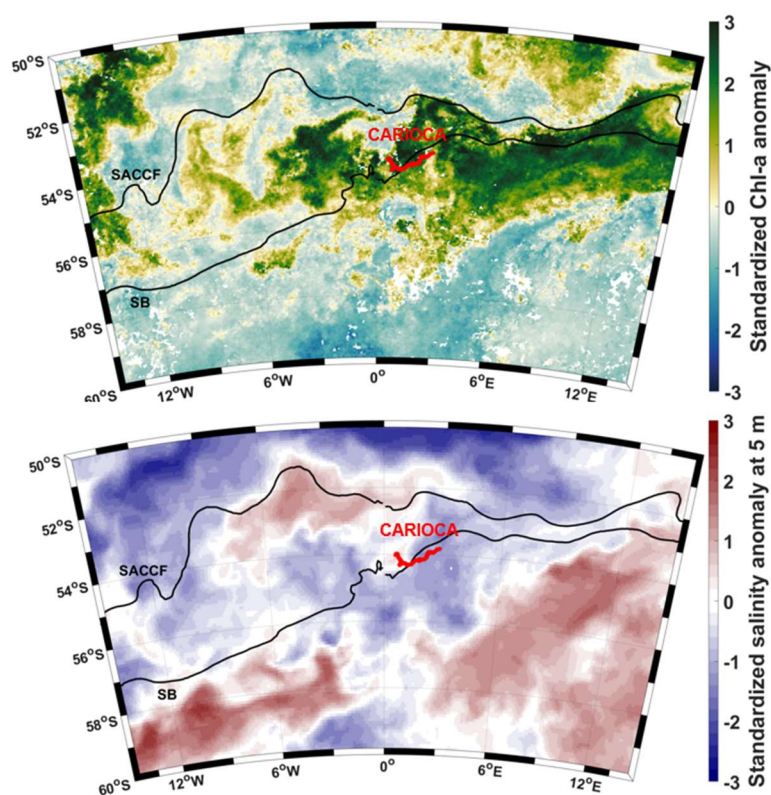


Figure 86: Anomalies in February 2022, relative to a 2011-2022 climatology, normalised with the standard deviation of monthly values for: (a). Top panel: Chl-a and (b)bottom panel: Salinity at 5 m using Mercator analysis. CARIOCA trajectory in February (red).

Moreover, the Lagrangian backward trajectories for the January-February 2022 bloom are not consistent with an origin from Bouvet Island or from seamounts, in contrast with the case in Sergi et al. (2020). Salinity in summer 2022 near CARIOCA was anomalously fresh (Fig. 6). Another possible source of iron fertilization could come from the melting of icebergs (Person et al., 2019). An analysis of satellite images enables us to rule out the hypothesis of iceberg melting in the vicinity of the CARIOCA drifter, or of water fertilised by the melting of the supergiant iceberg A68A (Smith and Bigg, 2023) that happened near South Georgia in Fall 2021, being the cause of the bloom. Although there were some iceberg fragments present near the CARIOCA after its deployment, in January 2022 (Fig. S2 in Supplement), the large size of the fresh water mass coming from the south-east, all point towards an export of fresh waters from the Weddell Sea. Salinity was anomalously fresh (Fig 8b), although there was no significant rainfall during that period at the position of the fresh water mass (not shown). Both salinity maps (from Mercator/Glorys (not shown) and backward trajectories enable us to track the travel of this fresh water mass, from its formation near the ice edge in spring 2021, to the position of the CARIOCA and glider, in summer 2022. The fresh water mass was formed near the sea ice edge (from September 2021 to November 2021, (Fig. C1). Indeed, in 2021, the ice retreated abnormally early, from September to mid-November 2021, anomalous north-eastward motion of sea ice was observed in the north-east Weddell Sea (Wang et al., 2022, their Fig. 3 and 4) and the austral summer 2022 marked a record for the lowest sea ice extent in Antarctica (Wang et al., 2022).

4.1 Impact of anomalous sea ice retreat on phytoplankton blooms

Previous studies have shown that the melting of sea ice can fertilize the region near the sea ice edge and stratify the water masses (Briggs et al., 2018; McClish and Bushinsky, 2023). Other factors such as light availability, grazing pressure and phytoplankton community composition should also be considered (Smith and Comiso, 2008, Briggs et al., 2018, Mc Clish and Bushinsky., 2023), and it has been shown that the date of sea ice breakup conditions the onset and magnitude of ice edge blooms (Mc Clish and Bushinsky., 2023). We can suppose that this is what the early sea ice retreat promoted the development of a phytoplankton bloom at the sea ice edge in spring 2021 (Fig. 5a4) (Wang et al., 2022). Model results of Death et al. (2014) also suggested that subglacial meltwaters may constitute a significant additional source of bioavailable iron to the Southern Ocean, supplementing iceberg sources, and that the impact of the glacial iron flux may be large, extending across much of the Southern Ocean due to the redistribution of the iron by ocean circulation.

We can thus infer/hypothesize that phytoplankton bloom near CARIOCA trajectory in January-February 2022 was favoured by stratified, fresher waters (Fig. 8b3 (a), 6 and D2) and micro nutrients supplied by ice melt and redistributed by ocean circulation. This is supported by fresh and enriched Chl-a water that detached from the sea ice edge region around 4°W in November 2021 and migrated north-westward (Fig. 54). This leads to the presence, in December 2021, of a patch of moderate Chl-a around 6°W, 57°S (Fig. 6D1) along the Lagrangian backward trajectory (Fig. E1 in Appendix 4). Then, this patch migrates north-eastward, and reaches the CARIOCA in January 2022, with Chl-a slightly higher than in December, possibly because of additional fertilization by nearby seamounts or because of the presence of different phytoplankton community composition. In March 2022, the waters reaching CARIOCA originated from farther south, closer to the ice (Fig. E1 in Appendix), then passed near

Bouvet Island,4) before reaching the CARIOCA (Fig. E14). Hence these waters might have been even more enriched in micro nutrients related to sea-ice melt. Also, as shown by previous studies, the proximity of Bouvet Island might have further fertilised the region (Sergi et al., 2020). This is consistent with the decrease in DIC and increase in Chl-a observed by CARIOCA from the beginning of March (Fig. 2).

4.2 Interannual variation

The backward trajectories show that waters near 0°S, 54°S in February, generally came from the south-west the previous years as well (Fig. S4not shown). We therefore investigate a possible link between the intensity of the bloom at the extremities of the Lagrangian backward trajectory between November and February, from 2010 to 2022, to study a possible link between spring blooms near the sea ice edge and summer blooms near Bouvet Island.

In spring 2021-summer 2022, the blooms at both extremities of the backward trajectories were much more pronounced than usual, with Chl-a concentrations above 1 mg.m⁻³ in both November 2021 (along the backward trajectory) and in February 2022 (along the CARIOCA trajectory) (Figure 97).

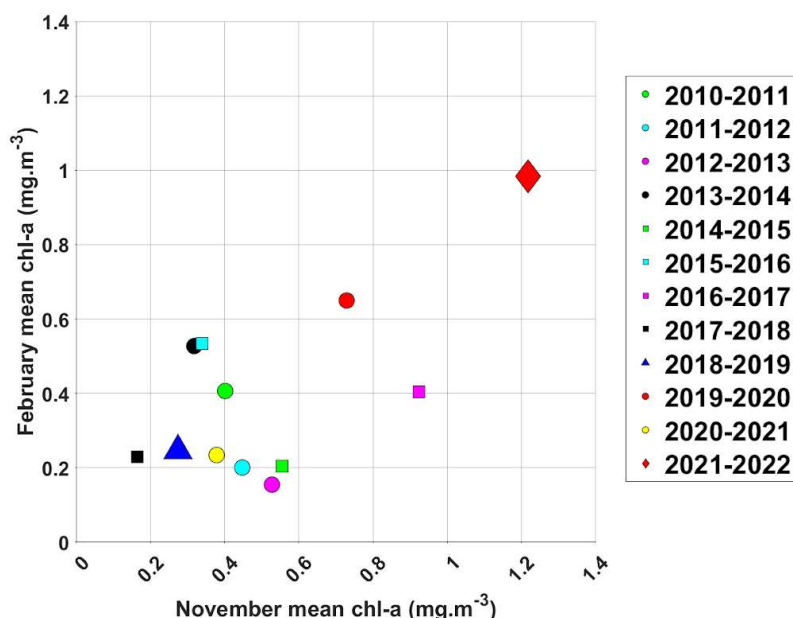


Figure 97: Mean Chl-a along CARIOCA position in February plotted against the mean Chl-a along the backward trajectories (computed using OSCAR currents) in November, for each year from 2010 to 2022.

This supports the hypothesis that there might be a link between the fertilization near the sea ice edge and the biological activity at the CARIOCA location. This also suggests that a strong spring bloom, promoted by near sea ice retreat, edge could promote the development of a strong summer bloom farther north. Following the same logic, when low concentrations of Chl-a were observed in November, similarly low concentrations of Chl-a were usually observed in February (see for instance 2018-2019, Fig. 97).

4.3 Interpretation of the low DIC and fCO₂ observed by CARIOCA fCO₂ measurements and derived DIC

During sea ice retreat, large net community production occurs in the seasonal ice zone (SIZ), likely due to iron delivery or low grazing rates (McClish and Bushinsky, 2023). Moreover, these authors found, based on BGC Argo

floats observations, that the bloom NCP increases in case of early sea ice retreat. Given that the water mass reaching the CARIOCA subpolar region remained in the bloom near sea ice edge from September to November 2021, i.e. over the whole bloom period, it seems reasonable to consider that the DIC of this water mass was affected by a bloom NCP typical of early ice retreat, of $3 \text{ mol C mol}^{-1} \text{ m}^{-2}$ (Figure 4 of McClish and Bushinsky, 2023) which would correspond to a $f\text{CO}_2$ as low as $240 \text{ } \mu\text{atm}$ (Appendix FE). Assuming that from end November 2021 to January 2022, the $f\text{CO}_2$ change along the water mass trajectory was only affected by air-sea exchange and temperature change, we estimate a $f\text{CO}_2$ of $342 \text{ } \mu\text{atm}$ at the end of January 2022 (see details in Appendix FE), a value very close to the one observed by CARIOCA (Figure 2a). In this crude estimation, we neglect biological production along the water mass trajectory and mixing with subsurface water. The latter seems at first order reasonable given that the salinity anomaly persisted along the water mass trajectory until January 2022. For what concerns the biological activity, the Chl-a was much lower along the water mass trajectory in December 2021-January 2022 than in the vicinity of the sea ice edge in spring 2021, suggesting low NCP. Moreover, the DIC derived from CARIOCA observations in January-February 2022 remained relatively stable (Fig. 2), at a low value, suggesting a balance between biological production and other processes, such as subsurface mixing or consumption by grazers. Our hypothesis is that the very low DIC and $f\text{CO}_2$ concentrations and highly negative CO_2 fluxes observed by the CARIOCA are not due to the local summer bloom in itself, but rather to a fresh water mass, already depleted in carbon, advected from the ice edge in November 2021 to the position of the buoy in summer 2022.

4.4 Study limits and perspectives

Another possible source of iron fertilization could come from the melting of icebergs (Person et al., 2019). An analysis of satellite images enables us to rule out the hypothesis of iceberg melting in the vicinity of the CARIOCA drifter, or of water fertilized by the melting of the supergiant iceberg A68A (Smith and Bigg, 2023) that happened near South Georgia in fall 2021, being the cause of the bloom. Although there was some iceberg fragments present near the CARIOCA after its deployment, in January 2022 (Fig. S3 in Supplement), the large size of the fresh water mass coming from the south-west, all point towards an export of fresh waters from the Weddell Sea.

Our ~~Chl-a~~ study was focused only on the region surrounding Bouvet Island, from 50° S to 60° S , and 15° W to 15° E . We could envision further studies on the impact of sea ice retreat at latitudes farther north, in the whole Southern Ocean, not just in the Atlantic sector. ~~The kind of analysis performed in this study could be extended on other islands in the Southern Ocean and see if the combined effect of sea ice retreat and fertilization from the island, could enhance phytoplankton development around other Southern Ocean islands.~~ The year 2022 was a record for lowest sea ice extent in austral summer (Wang et al., 2022). We could ~~hypothesize~~ hypothesize that ~~the~~ these fresh waters, already depleted in carbon, travelled farther north than usual, due to this unprecedented low sea ice extent record. It has been shown that due to global warming, there is a tendency for more sea ice retreat in the Southern Ocean in the future (Wang et al., 2022). ~~This could lead to stronger undersaturation of $f\text{CO}_2$ in regions usually in equilibrium with the atmosphere in austral summer. Phytoplankton travelling to 2022)~~ and for an increased northward freshwater transport (Haumann et al., 2016). This could lead to stronger undersaturation of $f\text{CO}_2$ and more negative CO_2 fluxes in regions usually in equilibrium with the atmosphere in austral summer. Anomalous large phytoplankton blooms at higher “northern” latitudes could also lead to a shift in the hunting zones of predators and might therefore have an impact on the ecosystem, in the long

term. Studies have shown that due to higher emissions and a warmer climate, there might be a change in the future location, mechanism and seasonality of the carbon sink in the Southern Ocean, with an increase of CO₂ uptake in certain regions (Hauck et al., 2015; Mongwe et al., 2024). In this context, events such as the one observed in summer 2022, that is, an increased sea ice retreat ~~leading to~~ and a north-eastward advection of a fresh water mass accompanied with a shift of the CO₂ sink to higher “northern” latitudes, ~~should~~ could become more frequent, and should be monitored carefully.

Vertical profiles provided by the glider were very useful to interpret CARIOCA surface measurements. Unfortunately, it was not possible to get additional vertical biogeochemical information from other platforms. Most of the BGC ARGO floats were too far away or didn't bring any additional information to our study. Our results highlight the sparsity of data in the subpolar region and their importance to constrain the Southern Ocean CO₂ flux.

5. Conclusion

Lagrangian backward trajectories suggest that the summer 2022 phytoplankton bloom in the subpolar ocean is mainly due to early sea ice retreat during the previous spring, and not due to the proximity of Bouvet Island or seamounts, as was the case in Sergi et al. (2020). ~~Although there~~ There was probably some ~~contribution,~~ fertilization in March 2022, due to ~~fertilization~~ the proximity of Bouvet Island. However, at the end of January 2022, the waters did not come from Bouvet Island, and the CARIOCA buoy was already in Chl-a rich waters, ~~at the end of January 2022, west of Bouvet. Indeed, the phytoplankton bloom in which the CARIOCA entered did not originate from Bouvet Island but coincides. This coincided~~ with the presence of a fresh water mass. ~~Mercator/Glorys salinity maps and Lagrangian backward trajectories, from November 2021 to March and a strong summer 2022, fCO₂ undersaturation. We show that this fresh water mass~~ the waters sampled by the buoy and the glider, originate from ~~the vicinity of sea ice edge, a region~~ south-west of the instruments' deployment, ~~at around in the vicinity of the sea ice edge (Fig. 4-5° W and 55.5-56.5° S).~~ Early sea ice retreat in spring 2021 ~~fuelled seawater with micro-nutrients leading to~~ promoted the development of a large phytoplankton bloom ~~near sea~~ at the ice edge, ~~which then travelled to the CARIOCA position. These waters were likely already. Waters~~ depleted in carbon ~~near sea ice edge when they escaped towards CARIOCA location which led to very undersaturated CARIOCA fCO₂.~~ This shows that productive waters from the sea ice edge travelled farther north than usual, up to 54° S, causing a strong undersaturation of fCO₂ and highly negative CO₂ fluxes in regions a region usually known to be in equilibrium with the atmosphere. (Gruber et al., 2019). Austral summer 2022 was a record for an unusually low sea ice extent (Wang et al., 2022). Our observations highlight the northward migration of the CO₂ sink associated with early sea ice retreat, a phenomenon projected by Earth System Models under climate change (Mongwe et al. 2024), with significant reduction in biologically-derived fCO₂ associated with melting ice, and the consequent increase in the oceanic CO₂ sink in certain sectors of the Southern Ocean.

Appendix A: Net Community Production (NCP) estimations

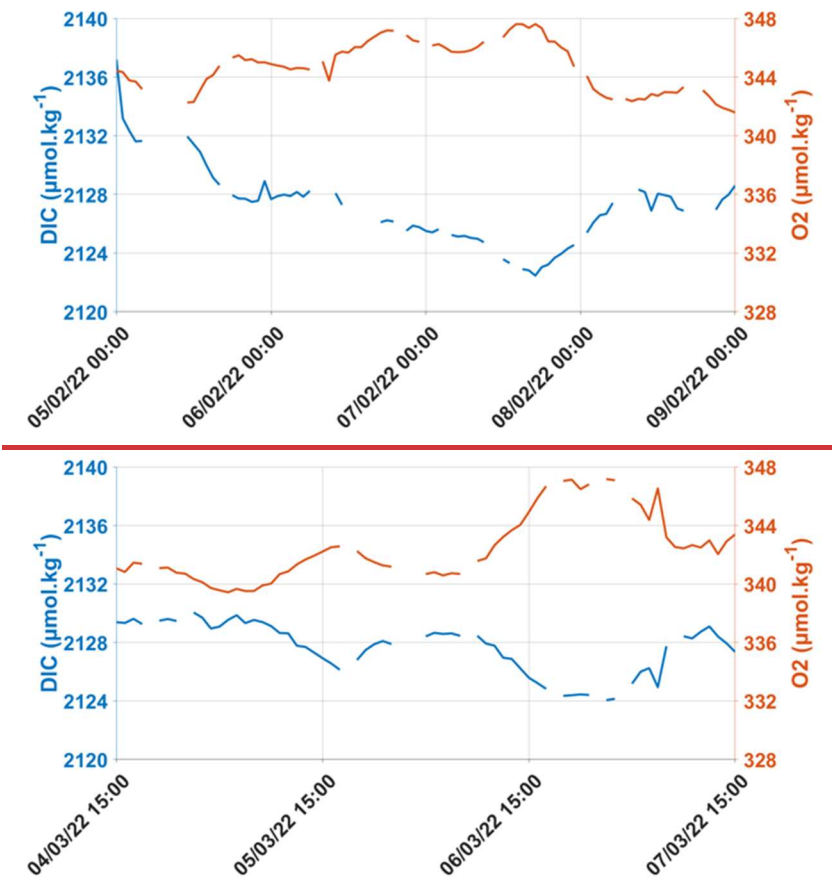


Figure A1: DIC and O₂ (uncorrected) for periods during which NCP was estimated, in summer 2022.

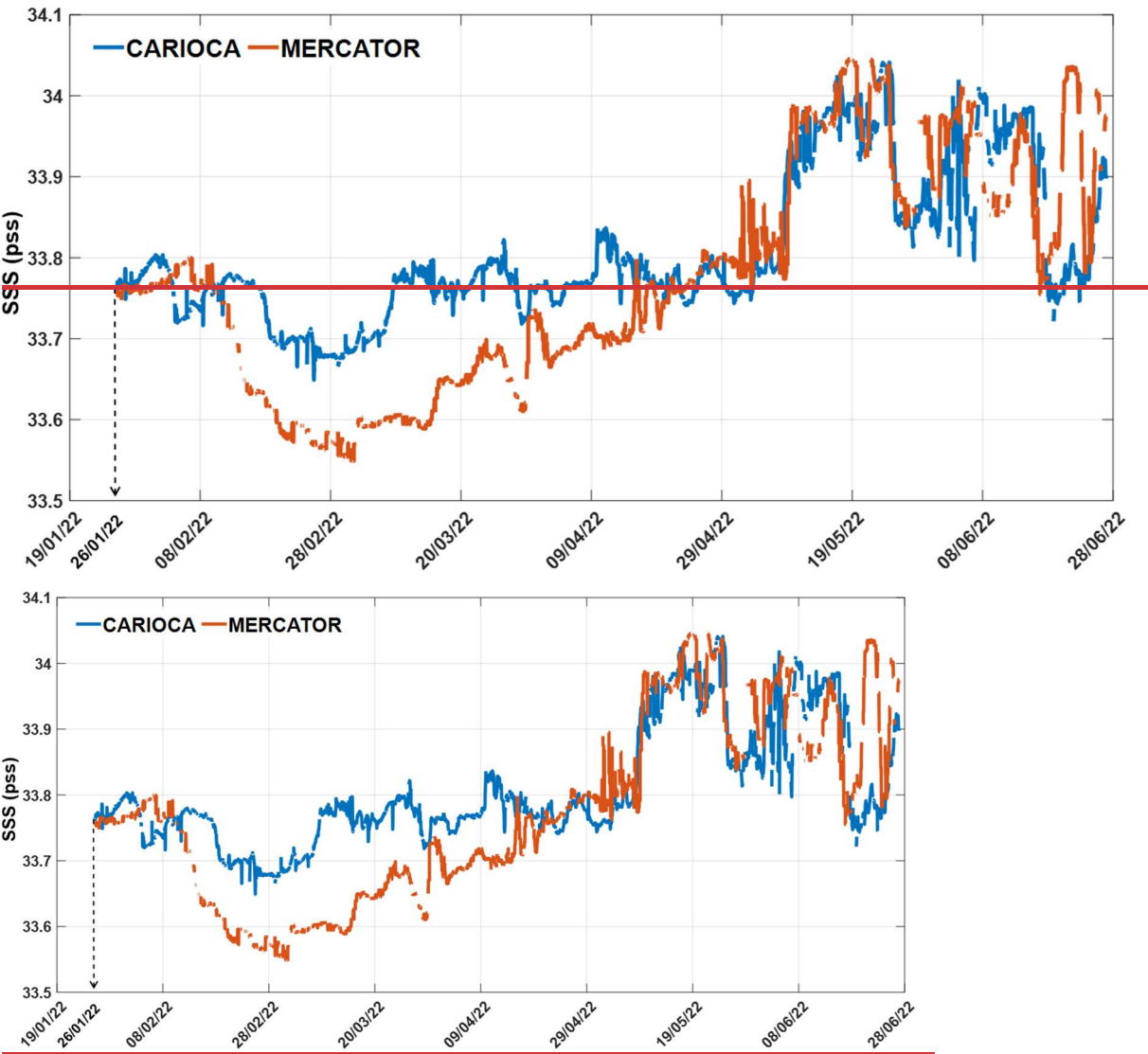
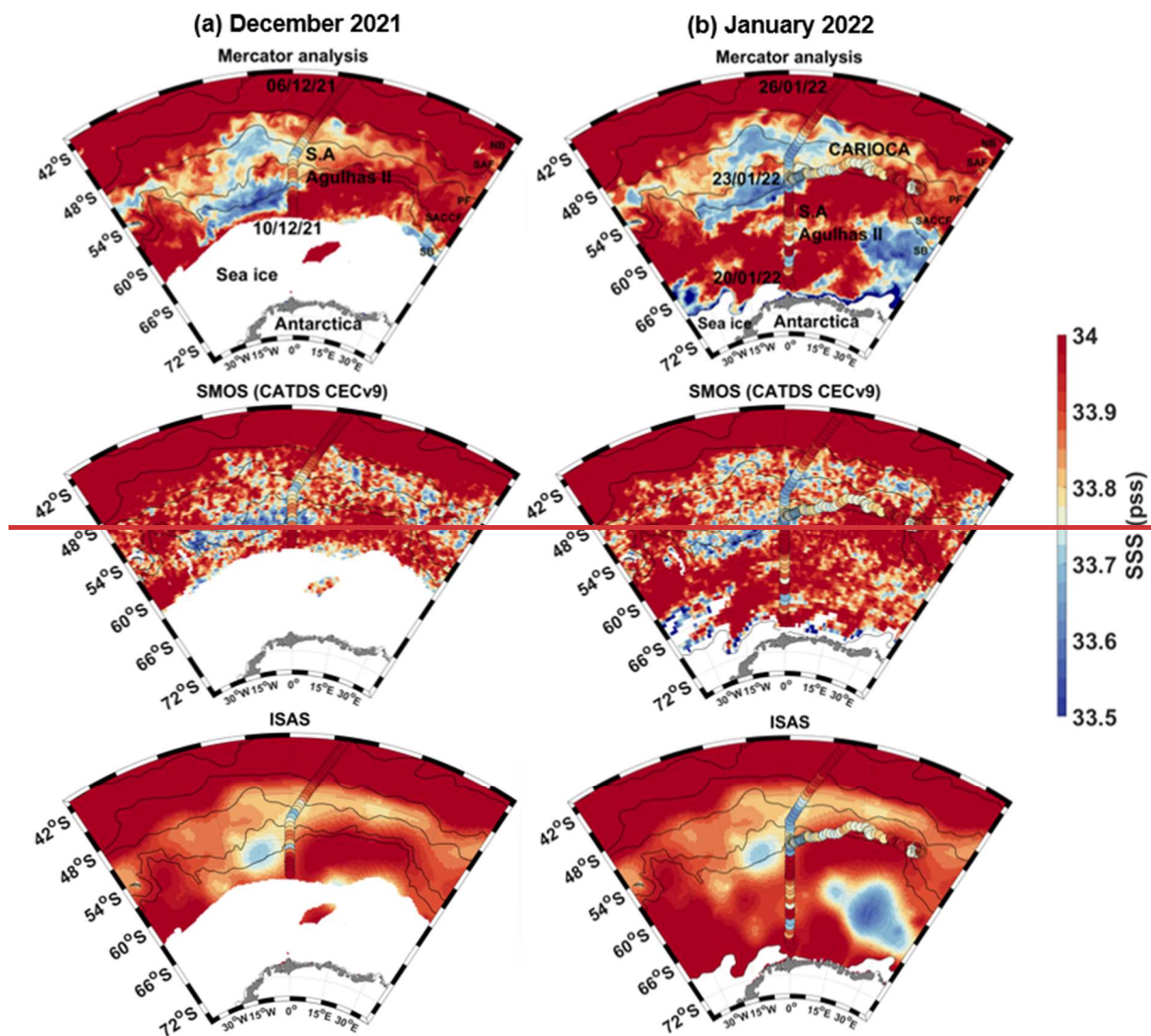


Figure B1A1: Colocalization between CARIOCA hourly SSS, at 2 m, colocated with and Mercator's daily salinity, at 5 m, from the 26 January to the 27 June 2022.



Appendix B: Net Community Production (NCP) estimations

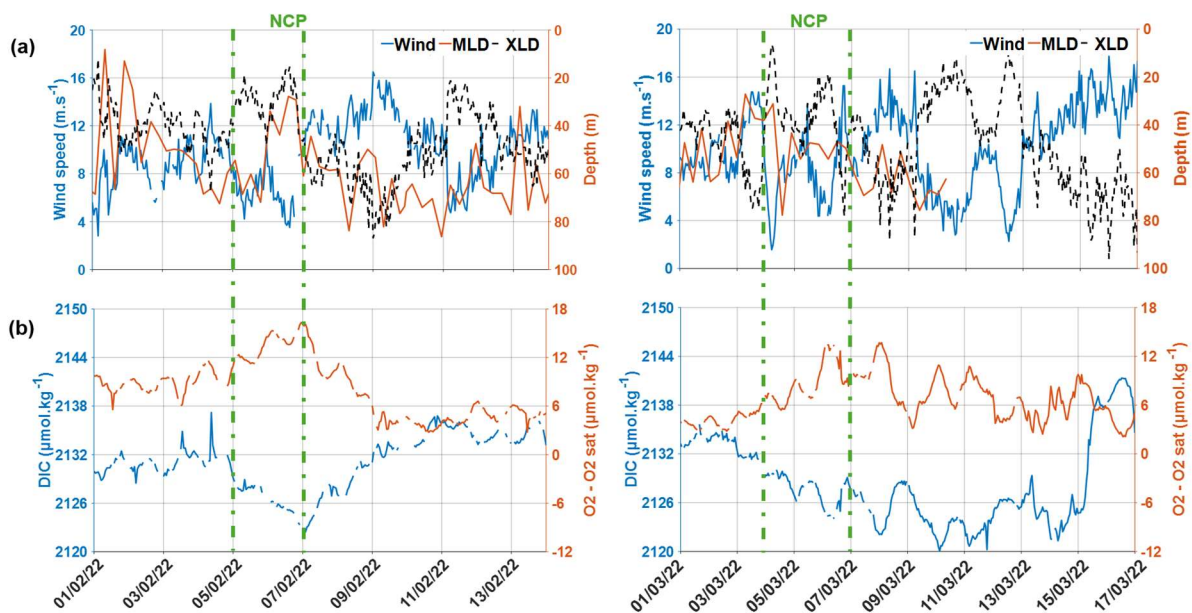


Figure B2B1: CARIOCA time series, during NCP periods on the 5-7 February 2022 (left), and on the 4-7 March 2022 (right), (a) Wind speed, MLD and XLD (b) DIC and O₂-O₂ sat.

Appendix C: Fresh water mass as detected by different salinity products

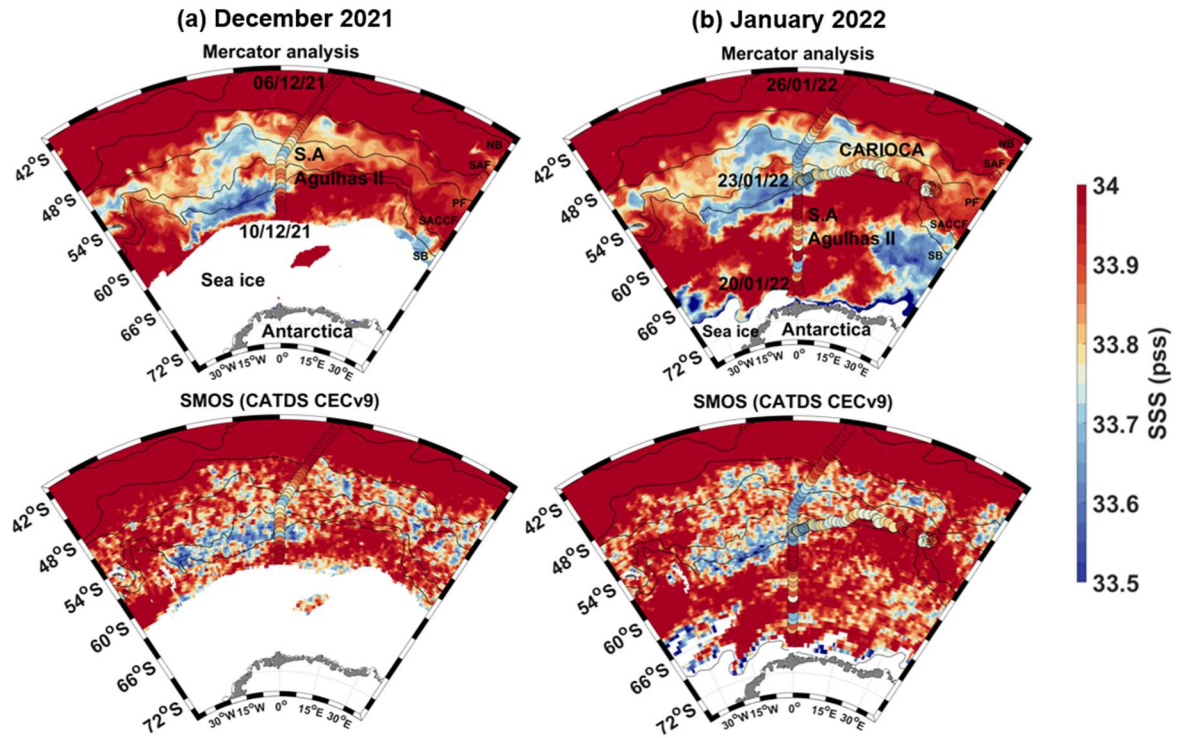


Figure C1: Mercator salinity at 5 m, and SMOS CATDS CECv9.0 SSS, and ISAS (MY) salinity at 5 m, with sea ice mask (0 % threshold of sea ice concentration) and fronts superimposed, (a) December 2021 mean SSS map, with S.A. Agulhas II SSS from the 6-10 December 2021, (b) January 2022 mean SSS map, with CARIOCA SSS from the 26 January 2022 to the 27 June 2022, and S.A. Agulhas II SSS from the 20-26 January 2022. SMOS SSS was adjusted by -0.1 pss to fit with CARIOCA and S.A. Agulhas II SSS.

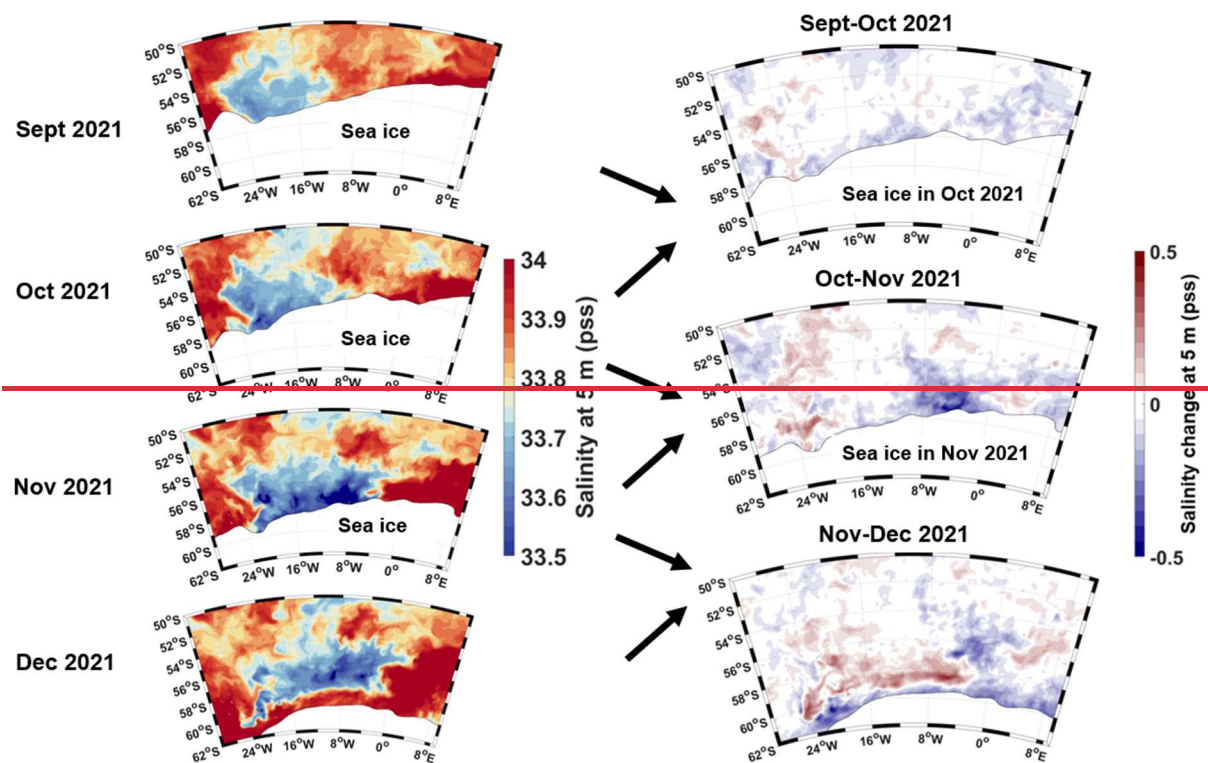
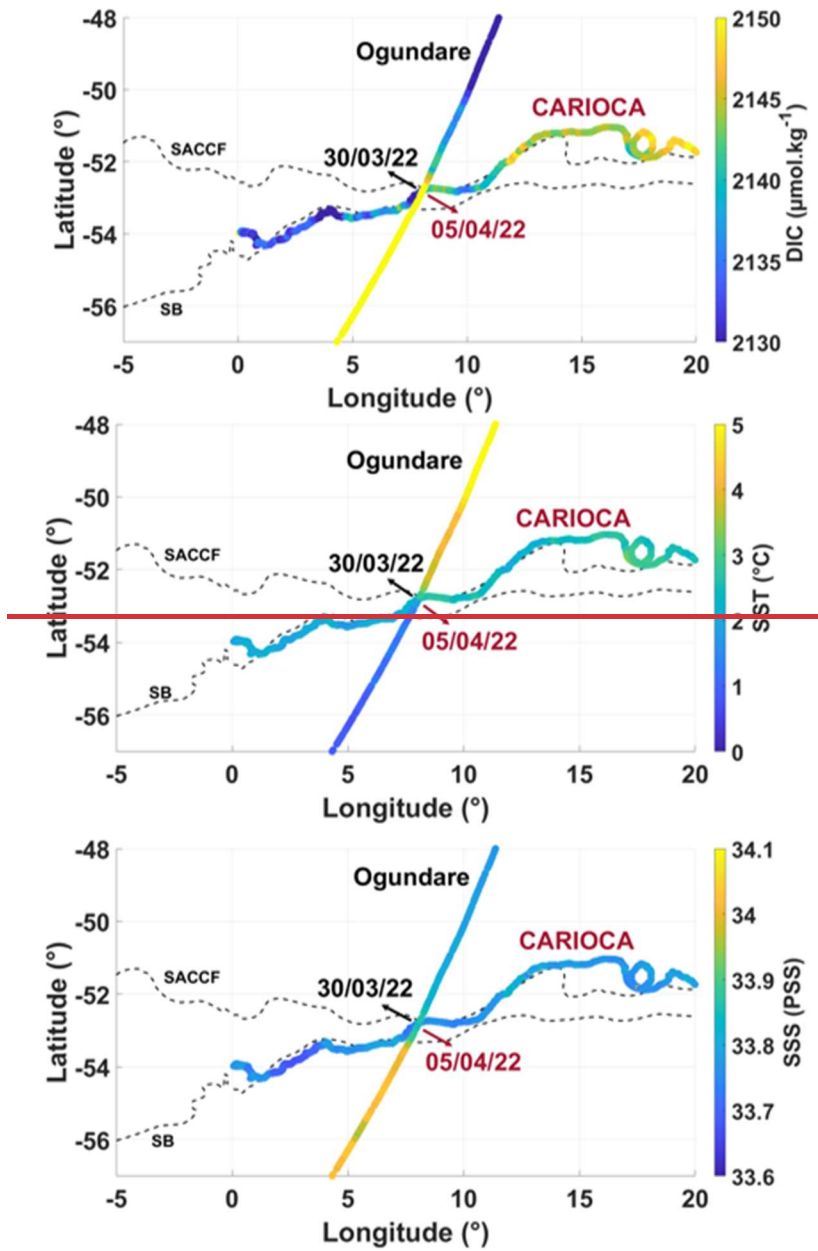


Figure C1: (a) Mercator salinity at 5 m, with sea ice (10 % threshold of sea ice concentration, from OSI SAF) receding from September to December 2021, (b) corresponding salinity change maps.

Appendix D: Comparison between summers 2022 and 2019

On 19 December 2018, a Wave Glider (a surface autonomous vehicle) was deployed, at 0° E, 54° S (Nicholson et al., 2022). It stayed fixed at this position for about two months, and performed surface measurements, until 11 February 2019. A comparison was made between this Wave Glider and the CARIOCA surface data. The CARIOCA stayed near 0° E, 54° S, from 26 January to 1 February 2022.

In 2019, the $f\text{CO}_2$ measured by the Wave Glider was near equilibrium with the atmosphere (2019 Wave Glider $f\text{CO}_2 \sim 410 \mu\text{atm}$) whereas the CARIOCA buoy measured a large CO_2 undersaturation (2022 CARIOCA $f\text{CO}_2 \sim 330 \mu\text{atm}$, Fig. 2a). In summer 2022 (from 26 January to 11 February 2022) the MLD was around 60 m, whereas in summer 2019 (from 19 December 2018 to 11 February 2019) the MLD was deeper, around 100 m (not shown). According to Nicholson's study, in 2019 the DIC concentration was around $2180 \mu\text{mol kg}^{-1}$, while in January to March 2022 it was much lower ($\sim 2130 \mu\text{mol kg}^{-1}$). After March, as the buoy went out of the Chl-a rich waters, the CARIOCA derived DIC increased gradually, until it reached concentrations around $2170 \mu\text{mol kg}^{-1}$ in June 2022 (Fig. 2 (b)), close to the ones measured by the Wave Glider in 2019.



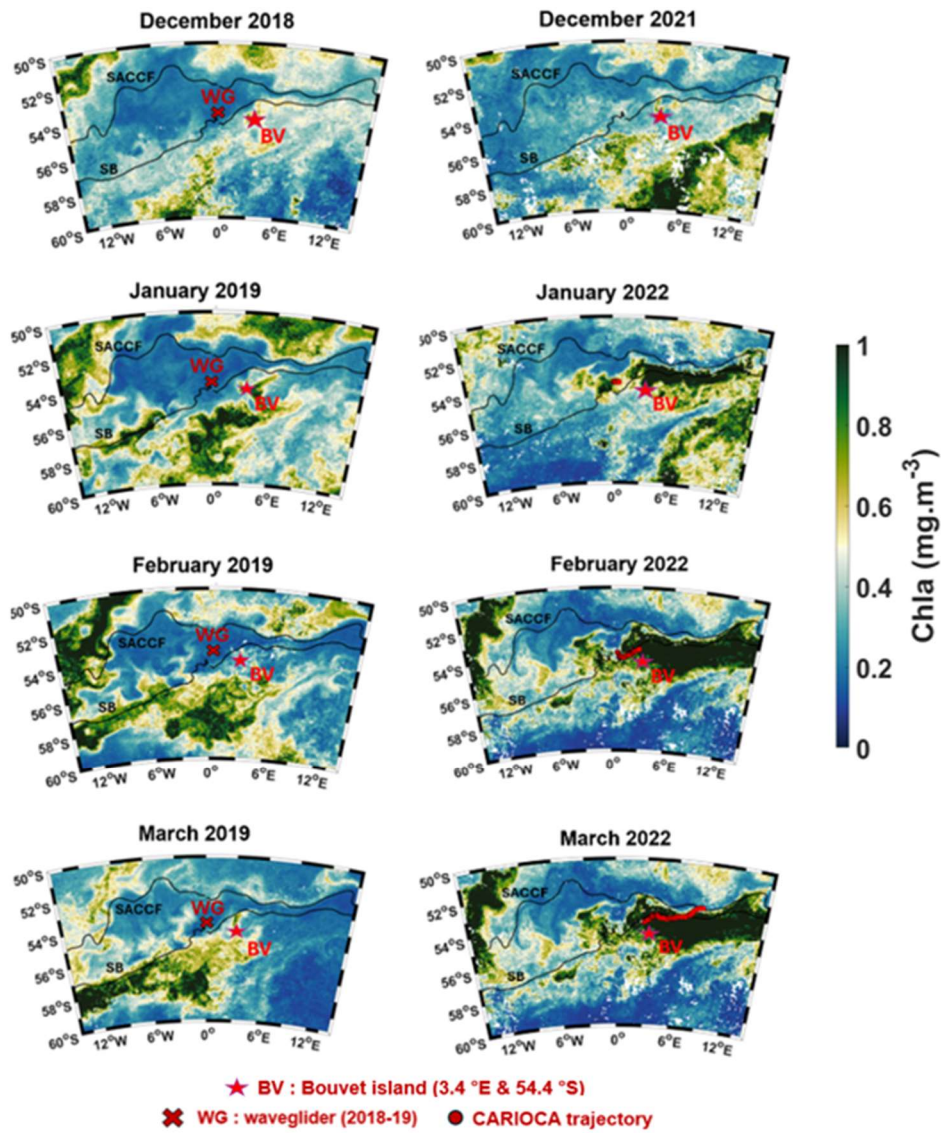


Figure D1: CCI Chl-a maps from December to March, left panel: 2018-2019, with Wave Glider position for the given month in red, right panel: same as left, but for 2021-2022, with CARIOCA position for the given month in red. (SB: Southern Boundary, SACCF: Southern Antarctic Circumpolar Current Front).

For the Chl-a comparison, CCI data were used to determine the Chl-a concentrations in the region in summer 2019 and 2022 (Fig. D1). From January to March 2022, a large phytoplankton bloom was observed around the Southern Boundary, at the CARIOCA position. This phytoplankton bloom was not present at the Wave Glider and CARIOCA locations, in summer 2019. Indeed, in January-March 2019, the bloom was farther south, south of the Southern Boundary (SB) (Fig. D1). The Chl-a concentrations were also lower in summer 2019 compared to 2022 and reached up to 1.5 mg m^{-3} in 2022, whereas in 2019, the maximum Chl-a concentrations did not exceed 1 mg m^{-3} .

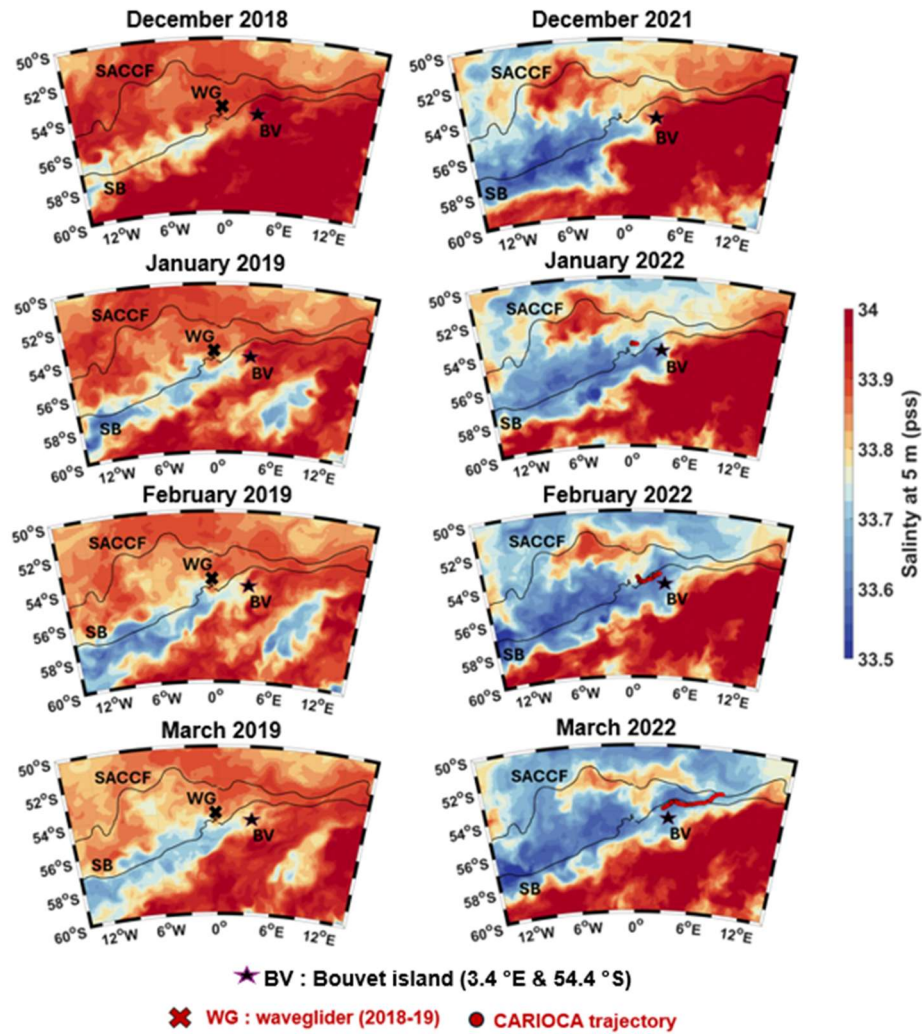


Figure D2: Sea Surface Salinity (SSS) at 5 m, from December to March, left panel: Glorlys SSS 2018-2019, with Wave Glider position for the given month in red, right panel: Mercator SSS 2021-2022, with CARIOCA position for the given month in red. (SB: Southern Boundary, SACCF: Subantarctic Circumpolar Current Front).

The phytoplankton bloom in summer 2022 in fact coincides with the presence of a fresh water mass. Mercator salinity profiles for spring 2021-summer 2022 (not shown), show that this lower salinity was only present in the first 60 m, which also corresponds to the glider salinity profile (Fig. 3). According to Glorlys, in 2019, the lower salinities were much farther south (Fig. D2).

A comparison was also performed with surface transects of the Norwegian RV *Kronprins Haakon* cruise from the 28 February 2019 to the 10 April 2019, (Ogundare et al., 2021). A ship transect crossed the CARIOCA path at around the same dates (end of March/beginning of April for both), for different years (2019 and 2022). North of the Southern Antarctic Circumpolar Current Front (SACCF), in April, the DIC, SST and SSS values for both years were consistent with each other. South of the SACCF, in 2019 the DIC concentration was higher ($\sim 2150 \mu\text{mol kg}^{-1}$) compared to the CARIOCA derived DIC concentration in 2022 (as low as $2120 \mu\text{mol kg}^{-1}$, South of the SACCF). The ship's path in 2019, south of the SACCF, was between $5-8^\circ \text{E}$ and $53-57^\circ \text{S}$. At these positions, in 2019, where higher salinities were measured (ship SSS ~ 34 pss, CARIOCA SSS ~ 33.7 pss, before April) (Fig. D3) and the Ch-a concentrations were lower, compared to 2022 (Fig. D1).

the Chl-a concentrations were low (Fig.). At these positions, higher salinities and temperatures were also measured by the RV *Kronpins Haakon*, in 2019 (SSS ~ 34 pss before April 2019) (Fig.

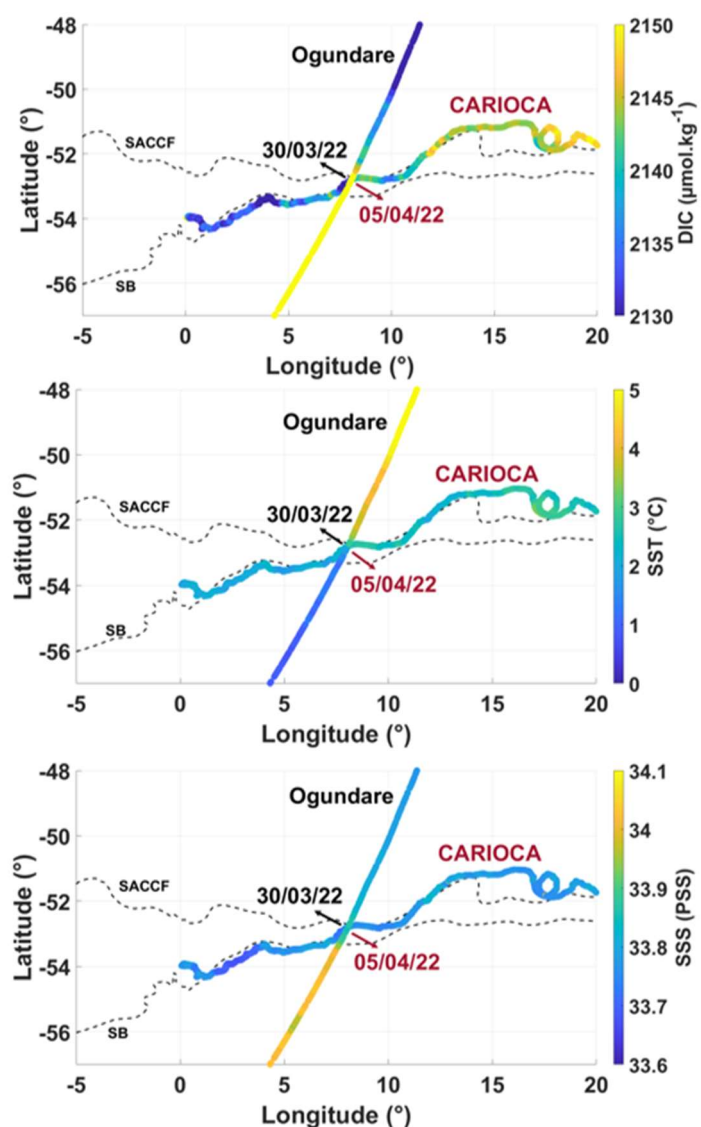


Figure D3: DIC, SST and SSS of CARIOCA SO-CHIC (2022) and Ogundare (2019).

Appendix E : Origin of summer 2022 phytoplankton bloom

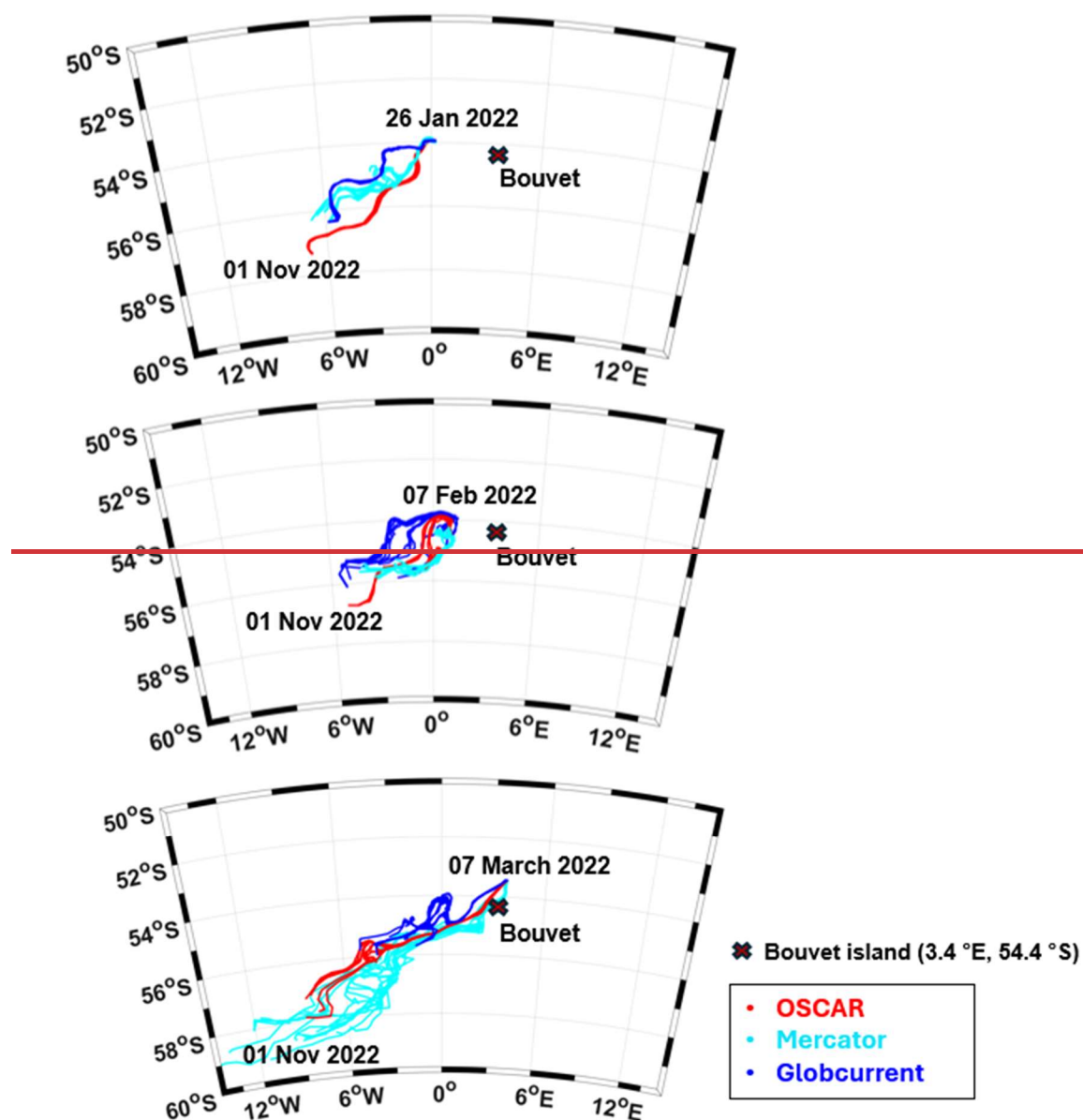


Figure E1: Backward trajectories from January, February, and March 2022 to November 2021, using different current products (Mercator analysis, OSCAR, Globcurrent).

Appendix F Appendix E: Estimation of DIC and fCO₂ variations along the water mass trajectory

Neglecting mixing and neglecting dfCO₂ due to salinity change,
the monthly changes of fCO₂ are estimated as in Merlivat et al. (2015):

$$\Delta fCO_2 = \Delta fCO_{2SST} + (\partial fCO_2 / \partial DIC) \Delta DIC \quad (F1)$$

With

$$dfCO_2/dt = (\partial fCO_2 / \partial T) dT/dt + (\partial fCO_2 / \partial DIC) dDIC/dt \quad (F2)$$

$$\partial fCO_2 / \partial T = (0.0423 \text{ } ^\circ\text{C}^{-1}) fCO_2 \quad (F3)$$

$$\partial fCO_2 / \partial DIC = R(fCO_2 / DIC), \text{ where } R \text{ is the Revelle factor} \quad (F4)$$

$$\text{Neglecting mixing: } \Delta DIC = \Delta DIC_{(bio)} + \Delta DIC_{(air-sea)} \quad (F5)$$

Where $\Delta DIC_{(bio)}$ is the contribution from biological production, and $\Delta DIC_{(air-sea)}$ is the contribution from the air-sea flux.

$$\Delta DIC_{(air-sea)} = F / (\rho * MLD), \text{ where } \rho \text{ is the seawater density and } F \text{ is the air-sea flux (Eq.(1))} \quad (F6)$$

We assume an exchange coefficient, K, of 0.1/12 mol m⁻² month⁻¹ μatm^{-1} (Boutin et al., 2009), and a Revelle factor, R, of 16 (Sabine et al., 2004).

According to (McClish and Bushinsky, 2023) the highest rates of daily net community production occur during active sea ice retreat and the bloom net community production is higher in case of early sea ice retreat. Given that the water mass reaching the CARIOCA subpolar region remained in the bloom near sea ice edge from September to November 2021, i.e. over the whole bloom period, it seems reasonable to consider that the DIC of this water mass was affected by a bloom NCP typical of early ice retreat, of 3 ~~mol~~ mol C m⁻² bloom⁻¹ (Figure 4 of McClish and Bushinsky, 2023). The MLD measured by the glider in summer 2022 is around 60 m. Assuming the same MLD depth in spring 2021, we estimate that the $\Delta DIC_{(bio)}$ due to the bloom near sea ice edge in spring 2021 was -50 $\mu\text{mol kg}^{-1}$. Assuming a DIC concentration before melting around 2200 $\mu\text{mol kg}^{-1}$ (Briggs et al., 2018) and fCO₂ initially in equilibrium with the atmosphere (fCO₂ ~ 400 μatm), the decrease in fCO₂ in November due to bloom NCP is estimated to be -160 μatm (November fCO₂ ~ 240 μatm).

We then assume that, at first order, the fCO₂ change along the water mass trajectory is only affected by air-sea exchange and temperature change (i.e. we neglect biological production along the water mass trajectory and mixing with subsurface water, which seems at first order reasonable given the relatively low Chl-a along the water mass trajectory than in the vicinity of the sea ice edge, and given that the salinity anomaly persisted along the water mass trajectory until January 2022 respectively).

From November 2021 to December 2021, $\Delta DIC_{(air-sea)} = 22 \text{ } \mu\text{mol kg}^{-1}$ and the $\partial fCO_{2(air-sea)}$ is +42 μatm . After the air-sea flux correction, we obtain a DIC concentration of about 2172 $\mu\text{mol kg}^{-1}$, and an fCO₂ of 282 μatm . The waters from sea ice melt are at -1.8 $^\circ\text{C}$ (seawater's freezing point). According to Remote Sensing System (REMSS, C.f. Data sets) and to backward trajectories, the SST along the water mass trajectory was -0.5 $^\circ\text{C}$ at the end of November 2021. Considering a heating of 1.3 $^\circ\text{C}$ ($\partial T = +1.3 \text{ } ^\circ\text{C}$) during the month of November, the temperature effect leads to an increase in fCO₂ of +15 μatm . At the end of December 2021, the fCO₂ is therefore 297 μatm .

In January 2022, $\Delta DIC_{(air-sea)}$ is +14 $\mu\text{mol kg}^{-1}$, and the $\partial fCO_{2(air-sea)}$ is +31 μatm . After the air-sea flux correction the fCO₂ is 328 μatm and the DIC is 2186 $\mu\text{mol kg}^{-1}$. According to REMSS and to backward trajectories, ∂T is +1.0 $^\circ\text{C}$, the $\partial fCO_{2(SST)}$ is 14 μatm . At the end of January 2021, the fCO₂ estimate is therefore 342 μatm .

Data Availability

All data used in this study are freely available and downloadable from the following websites. CARIOCA dataset is available on SEANOE at (<https://doi.org/10.17882/100800>, Naëck et al., 2024). The Seaglider (675SG675) dataset is available online at (<https://doi.org/10.5281/zenodo.11059426>, Swart et al., 2024). The *S.A Agulhas II* SO-CHIC 2022 cruise TSG dataset is available on SEANOE at (<https://doi.org/10.17882/100905>, Ward et al., 2024). The *S.A. Agulhas II* SO-CHIC 2022 cruise, CTD data is available on SEANOE at (<https://doi.org/10.17882/95314>, Steiger et al., 2022). ERA5 atmospheric pressure and wind speed hourly data on single levels from 1940 to present is available on Copernicus Climate Change Service Climate Data Store, at <https://doi.org/10.24381/cds.adbb2d47>. The « Global Ocean Physics Reanalysis » and the « Global Ocean Physics Analysis and Forecast » datasets are available on Copernicus Marine at <https://doi.org/10.48670/moi-00021> and <https://doi.org/10.48670/moi-00016>. The SMOS CATDS CECv9 salinity dataset is available online at <https://doi.org/10.17882/52804#102161>. The ISAS MultiYear salinity dataset is available on the data store of Copernicus Marine, at <https://doi.org/10.17882/46219>. The OSCAR dataset is available at <https://doi.org/10.5067/OSCAR-03D01>. The Globcurrent dataset is available at <https://doi.org/10.48670/mds-00327>. The OCI-CCI chlorophyll-a dataset is available online at <http://www.oceancolour.org>. The MW OI SST dataset produced by Remote Sensing Systems is available online at www.remss.com. The datasets “Global Sea Ice Concentration Climate Data Record v3.0 - Multimission, EUMETSAT SAF on Ocean and Sea Ice” and “Global Sea Ice Concentration Interim Climate Data Record Release 3 - DMSP, EUMETSAT SAF on Ocean and Sea Ice” are available online at http://doi.org/10.15770/EUM_SAF_OSI_0013 and http://doi.org/10.15770/EUM_SAF_OSI_0014. The SPASSO package containing the LAMTA software used for the lagrangian analysis can be downloaded at <https://www.swot-adac.org/resources/spasso/>

Supplement

The supplement related to this article is joined as a separate file to this submission.

Author contributions

K.Naëck conducted the data processing, analyzed the results, did the estimations, and wrote the paper. J.Boutin ~~oversawsupervised~~ the study, and helped in the data processing, ~~in the estimations, in the analysis and~~ interpretation of the results, estimations, and ~~in the paper's~~ conception ~~of the paper~~. S.Swart and M.du Plessis provided the Seaglider (675SG675) dataset. They also provided useful input concerning the Seaglider data processing and interpretation of the results. L.Merlivat provided useful inputs and insights during the progress of this study, suggesting various hypotheses and helping us investigate them. L.Beaumont oversaw the verification of the calibration of CARIOCA sensors. A.Lourenco helped in the deployment of the CARIOCA buoy during the SO-CHIC 2022 cruise. Their involvement during the COVID period enabled us to collect data vital to this study. F.d'Ovidio and L.Rousselet provided the python code used for the Lagrangian analysis, which is the basis of our study and without which we couldn't have proved the origin of the phytoplankton bloom. They helped with discussions and modifications related to this code, for our specific study case. B.Ward provided the TSG data of the *S.A. Agulhas II* ship (SO-CHIC 2022). J.B.Sallée coordinated the SO-CHIC project, and provided part of the financial support. All co-authors discussed, reviewed, and edited the paper.

Competing interests

The contact author has declared that none of the authors has any competing interests.

Acknowledgements

The authors would like to thank Dmitry Khvorostyanov (dimitry.khvorostyanov@locean.ipsl.fr) and Alain Laupin-Vinatier (alain.laupin-vinatier@locean.ipsl.fr) for the automation of CARIOCA data processing chain in real time. We also thank F.Bonjean, S.Nicholson and M.Vancoppenolle for helpful discussions. We also thank all those involved with the deployments of the CARIOCA buoy and glider during the SO-CHIC cruise on the RV SA Agulhas II.

Financial support

This project ~~has been partly funded by~~ is supported by funding from the European Union's Horizon 2020 Research and Innovation Program under grant agreement No. 821001 (SO-CHIC programme). L. Rousselet is supported by the CNES TOSCA Bioswot-AdAC project. S.Swart is supported by a Wallenberg Academy Fellowship (WAF 2015.0186) and the Swedish Research Council (VR 2019-04400).

References

- Ardaya, M., Lacour, L., Sergi, S., d'Ovidio, F., Sallée, J.-B., Rembauville, M., Blain, S., Tagliabue, A., Schlitzer, R., Jeandel, C., Arrigo, K. R., and Claustre, H.: Hydrothermal vents trigger massive phytoplankton blooms in the Southern Ocean, *Nat. Commun.*, 10, 2451, <https://doi.org/10.1038/s41467-019-09973-6>, 2019.
- Bakker, D. C. E., Pfeil, B., Landa, C. S., Metzl, N., O'Brien, K. M., Olsen, A., Smith, K., Cosca, C., Harasawa, S., Jones, S. D., Nakaoka, S., Nojiri, Y., Schuster, U., Steinhoff, T., Sweeney, C., Takahashi, T., Tilbrook, B., Wada, C., Wanninkhof, R., Alin, S. R., Balestrini, C. F., Barbero, L., Bates, N. R., Bianchi, A. A., Bonou, F., Boutin, J., Bozec, Y., Burger, E. F., Cai, W.-J., Castle, R. D., Chen, L., Chierici, M., Currie, K., Evans, W., Featherstone, C., Feely, R. A., Fransson, A., Goyet, C., Greenwood, N., Gregor, L., Hankin, S., Hardman-Mountford, N. J., Harlay, J., Hauck, J., Hoppema, M., Humphreys, M. P., Hunt, C. W., Huss, B., Ibáñez, J. S. P., Johannessen, T., Keeling, R., Kitidis, V., Körtzinger, A., Kozyr, A., Krasakopoulou, E., Kuwata, A., Landschützer, P., Lauvset, S. K., Lefèvre, N., Lo Monaco, C., Manke, A., Mathis, J. T., Merlivat, L., Millero, F. J., Monteiro, P. M. S., Munro, D. R., Murata, A., Newberger, T., Omar, A. M., Ono, T., Paterson, K., Pearce, D., Pierrot, D., Robbins, L. L., Saito, S., Salisbury, J., Schlitzer, R., Schneider, B., Schweitzer, R., Sieger, R., Skjelvan, I., Sullivan, K. F., Sutherland, S. C., Sutton, A. J., Tadokoro, K., Telszewski, M., Tuma, M., van Heuven, S. M. A. C., Vandemark, D., Ward, B., Watson, A. J., and Xu, S.: A multi-decade record of high-quality $f\text{CO}_2$ data in version 3 of the Surface Ocean CO_2 Atlas (SOCAT), *Earth Syst. Sci. Data*, 8, 383–413, <https://doi.org/10.5194/essd-8-383-2016>, 2016.
- Blain, S., Quéguiner, B., Armand, L., Belviso, S., Bombled, B., Bopp, L., Bowie, A., Brunet, C., Brussaard, C., Carlotti, F., Christaki, U., Corbière, A., Durand, I., Ebersbach, F., Fuda, J.-L., Garcia, N., Gerringa, L., Griffiths, B., Guigue, C., Guillermin, C., Jacquet, S., Jeandel, C., Laan, P., Lefèvre, D., Lo Monaco, C., Malits, A., Mosseri, J., Obernosterer, I., Park, Y.-H., Picherl, M., Pondaven, P., Remenyi, T., Sandroni, V., Sarthou, G., Savoye, N., Scouarnec, L., Souhaut, M., Thuiller, D., Timmermans, K., Trull, T., Uitz, J., van Beek, P., Veldhuis, M., Vincent, D., Viollier, E., Vong, L., and Wagener, T.: Effect of natural iron fertilization on carbon sequestration in the Southern Ocean, *Nature*, 446, 1070–1074, <https://doi.org/10.1038/nature05700>, 2007.
- Blain, S., Sarthou, G., and Laan, P.: Distribution of dissolved iron during the natural iron-fertilization experiment KEOPS (Kerguelen Plateau, Southern Ocean), *Deep Sea Res. Part II Top. Stud. Oceanogr.*, 55, 594–605, <https://doi.org/10.1016/j.dsr2.2007.12.028>, 2008.
- Boutin, J., Merlivat, L., HÉnocq, C., Martin, N., and Sallée, J. B.: Air-sea CO_2 flux variability in frontal regions of the Southern Ocean from CARbon Interface OCEan Atmosphere drifters, *Limnol. Oceanogr.*, 53, 2062–2079, https://doi.org/10.4319/lo.2008.53.5_part_2.2062, 2008.

769 Boutin, J., Quilfen, Y., Merlivat, L., and Piolle, J. F.: Global average of air-sea CO₂ transfer velocity from
770 QuikSCAT scatterometer wind speeds, *J. Geophys. Res. Oceans*, 114, <https://doi.org/10.1029/2007JC004168>,
771 2009.

772 Boutin, J., Vergely, J.-L., Khvorostyanov, D., and Supply, A.: SMOS SSS L3 maps generated by CATDS CEC
773 LOCEAN. debias V8.0, <https://doi.org/10.17882/52804>, 2023.

774 Boyd, P.W., Doney, S. C., Strzepek, R., Dusenberry, J., Lindsay, K., and Fung, I., Southern Ocean phytoplankton
775 and climate change, *Clim. Change*, 2007.

776 Briggs, E. M., Martz, T. R., Talley, L. D., Mazloff, M. R., and Johnson, K. S.: Physical and Biological Drivers of
777 Biogeochemical Tracers Within the Seasonal Sea Ice Zone of the Southern Ocean From Profiling Floats, *J.*
778 *Geophys. Res. Oceans*, 123, 746–758, <https://doi.org/10.1002/2017JC012846>, 2018.

779 Copin-Montégut, C., Bégovic, M., and Merlivat, L.: Variability of the partial pressure of CO₂ on diel to annual
780 time scales in the Northwestern Mediterranean Sea, *Mar. Chem.*, 85, 169–189,
781 <https://doi.org/10.1016/j.marchem.2003.10.005>, 2004.

782 C3S: ERA5 hourly data on single levels from 1940 to present, <https://doi.org/10.24381/CDS.ADBB2D47>, 2018.

783 de Boyer Montégut, C., Madec, G., Fischer, A. S., Lazar, A., and Iudicone, D.: Mixed layer depth over the global
784 ocean: An examination of profile data and a profile-based climatology, *J. Geophys. Res. Oceans*, 109,
785 <https://doi.org/10.1029/2004JC002378>, 2004.

786 Death, R., Wadham, J. L., Monteiro, F., Le Brocq, A. M., Tranter, M., Ridgwell, A., Dutkiewicz, S., and Raiswell,
787 R.: Antarctic ice sheet fertilises the Southern Ocean, *Biogeosciences*, 11, 2635–2643, [https://doi.org/10.5194/bg-](https://doi.org/10.5194/bg-11-2635-2014)
788 11-2635-2014, 2014.

789 DeVries, T.: The oceanic anthropogenic CO₂ sink: Storage, air-sea fluxes, and transports over the industrial era,
790 *Glob. Biogeochem. Cycles*, 28, 631–647, <https://doi.org/10.1002/2013GB004739>, 2014.

791 d'Ovidio, F., Della Penna, A., Trull, T.W., Nencioli, F., Pujol, M.-I., Rio, M.-H., Park, Y.-H., Cotté, C., Zhou, M.,
792 and Blain, S. (2015). The biogeochemical structuring role of horizontal stirring: Lagrangian perspectives on iron
793 delivery downstream of the Kerguelen plateau. *Biogeosciences* 12, 5567–5581.

794 EUMETSAT - Product Navigator - Global Sea Ice Concentration Climate Data Record v3.0 - Multimission:
795 <https://navigator.eumetsat.int/product/EO:EUM:DAT:0826>, last access: 10 July 2024.

796 EUMETSAT - Product Navigator - Global Sea Ice Concentration Interim Climate Data Record Release 3 - DMSP:
797 <https://navigator.eumetsat.int/product/EO:EUM:DAT:0645>, last access: 10 July 2024.

798 Friedlingstein, P., O'Sullivan, M., Jones, M. W., Andrew, R. M., Bakker, D. C. E., Hauck, J., Landschützer, P.,
799 Le Quéré, C., Luijkx, I. T., Peters, G. P., Peters, W., Pongratz, J., Schwingshackl, C., Sitch, S., Canadell, J. G.,
800 Ciais, P., Jackson, R. B., Alin, S. R., Anthoni, P., Barbero, L., Bates, N. R., Becker, M., Bellouin, N., Decharme,
801 B., Bopp, L., Brasika, I. B. M., Cadule, P., Chamberlain, M. A., Chandra, N., Chau, T.-T.-T., Chevallier, F., Chini,
802 L. P., Cronin, M., Dou, X., Enyo, K., Evans, W., Falk, S., Feely, R. A., Feng, L., Ford, D. J., Gasser, T., Ghattas,
803 J., Gkritzalis, T., Grassi, G., Gregor, L., Gruber, N., Gürses, Ö., Harris, I., Hefner, M., Heinke, J., Houghton, R.
804 A., Hurtt, G. C., Iida, Y., Ilyina, T., Jacobson, A. R., Jain, A., Jarníková, T., Jersild, A., Jiang, F., Jin, Z., Joos, F.,
805 Kato, E., Keeling, R. F., Kennedy, D., Klein Goldewijk, K., Knauer, J., Korsbakken, J. I., Körtzinger, A., Lan, X.,
806 Lefèvre, N., Li, H., Liu, J., Liu, Z., Ma, L., Marland, G., Mayot, N., McGuire, P. C., McKinley, G. A., Meyer, G.,
807 Morgan, E. J., Munro, D. R., Nakaoka, S.-I., Niwa, Y., O'Brien, K. M., Olsen, A., Omar, A. M., Ono, T., Paulsen,
808 M., Pierrot, D., Pocock, K., Poulter, B., Powis, C. M., Rehder, G., Resplandy, L., Robertson, E., Rödenbeck, C.,
809 Rosan, T. M., Schwinger, J., Séférian, R., et al.: Global Carbon Budget 2023, *Earth Syst. Sci. Data*, 15, 5301–
810 5369, <https://doi.org/10.5194/essd-15-5301-2023>, 2023.

811 Frölicher, T. L., Sarmiento, J. L., Paynter, D. J., Dunne, J. P., Krasting, J. P., and Winton, M.: Dominance of the
812 Southern Ocean in Anthropogenic Carbon and Heat Uptake in CMIP5 Models, *J. Clim.*, 28, 862–886,
813 <https://doi.org/10.1175/JCLI-D-14-00117.1>, 2015.

814 Giddy, I. S., Nicholson, S.-A., Queste, B. Y., Thomalla, S., and Swart, S.: Sea-Ice Impacts Inter-Annual Variability
815 of Phytoplankton Bloom Characteristics and Carbon Export in the Weddell Sea, *Geophys. Res. Lett.*, 50,
816 e2023GL103695, <https://doi.org/10.1029/2023GL103695>, 2023.

817 Giunta, V., & Ward, B. (2022). Ocean mixed layer depth from dissipation. *Journal of Geophysical Research:*
818 *Oceans*, 127, e2021JC017904. <https://doi.org/10.1029/2021JC017904>

819 Global Ocean Physics Analysis and Forecast:
820 https://data.marine.copernicus.eu/product/GLOBAL_ANALYSISFORECAST_PHY_001_024/description, last
821 access: 10 July 2024.

822 Global Ocean Physics Reanalysis:
823 https://data.marine.copernicus.eu/product/GLOBAL_MULTIYEAR_PHY_001_030/description, last access: 10
824 July 2024.

825 Global Total (COPERNICUS-GLOBCURRENT), Ekman and Geostrophic currents at the Surface and 15m:
826 https://data.marine.copernicus.eu/product/MULTIOBS_GLO_PHY_MYNRT_015_003/description, last access:
827 10 July 2024.

828 Gregor, L., Ryan-Keogh, T. J., Nicholson, S.-A., du Plessis, M., Giddy, I., and Swart, S.: GliderTools: A Python
829 Toolbox for Processing Underwater Glider Data, *Front. Mar. Sci.*, 6, <https://doi.org/10.3389/fmars.2019.00738>,
830 2019.

831 Gruber, N., Landschützer, P., and Lovenduski, N. S.: The Variable Southern Ocean Carbon Sink, *Annu. Rev. Mar.*
832 *Sci.*, 11, 159–186, <https://doi.org/10.1146/annurev-marine-121916-063407>, 2019.

833 Hauck, J., Völker, C., Wolf-Gladrow, D. A., Laufkötter, C., Vogt, M., Aumont, O., Bopp, L., Buitenhuis, E. T.,
834 Doney, S. C., Dunne, J., Gruber, N., Hashioka, T., John, J., Quéré, C. L., Lima, I. D., Nakano, H., Séférian, R.,
835 and Totterdell, I.: On the Southern Ocean CO₂ uptake and the role of the biological carbon pump in the 21st
836 century, *Glob. Biogeochem. Cycles*, 29, 1451–1470, <https://doi.org/10.1002/2015GB005140>, 2015.

837 Hauck, J., Nissen, C., Landschützer, P., Rödenbeck, C., Bushinsky, S., and Olsen, A.: Sparse observations induce
838 large biases in estimates of the global ocean CO₂ sink: an ocean model subsampling experiment, *Philos. Trans.*
839 *R. Soc. Math. Phys. Eng. Sci.*, 381, 20220063, <https://doi.org/10.1098/rsta.2022.0063>, 2023.

840 [Haumann, F. A., Gruber, N., Münnich, M., Frenger, I., and Kern, S.: Sea-ice transport driving Southern Ocean](#)
841 [salinity and its recent trends, *Nature*, 537, 89–92, <https://doi.org/10.1038/nature19101>, 2016.](#)

842 Henley, S. F., Cavan, E. L., Fawcett, S. E., Kerr, R., Monteiro, T., Sherrell, R. M., Bowie, A. R., Boyd, P. W.,
843 Barnes, D. K. A., Schloss, I. R., Marshall, T., Flynn, R., and Smith, S.: Changing Biogeochemistry of the Southern
844 Ocean and Its Ecosystem Implications, *Front. Mar. Sci.* 7, 581, <https://doi.org/10.3389/fmars.2020.00581>, 2020.

845 Holte, J. and Talley, L.: A New Algorithm for Finding Mixed Layer Depths with Applications to Argo Data and
846 Subantarctic Mode Water Formation*, *J. Atmospheric Ocean. Technol.*, 26, 1920–1939,
847 <https://doi.org/10.1175/2009JTECHO543.1>, 2009.

848 Laws, E. A.: Photosynthetic quotients, new production and net community production in the open ocean, *Deep*
849 *Sea Res. Part Oceanogr. Res. Pap.*, 38, 143–167, [https://doi.org/10.1016/0198-0149\(91\)90059-O](https://doi.org/10.1016/0198-0149(91)90059-O), 1991.

850 [Landschützer, P., Gruber, N., Haumann, F. A., Rödenbeck, C., Bakker, D. C. E., Van Heuven, S., Hoppema, M.,](#)
851 [Metzl, N., Sweeney, C., Takahashi, T., Tilbrook, B., and Wanninkhof, R.: The reinvigoration of the Southern](#)
852 [Ocean carbon sink, *Science*, 349, 1221–1224, <https://doi.org/10.1126/science.aab2620>, 2015.](#)

853 [Lannuzel, D., Vancoppenolle, M., van der Merwe, P., de Jong, J., Meiners, K. M., Grotti, M., Nishioka, J., and](#)
854 [Schoemann, V.: Iron in sea ice: Review and new insights, *Elem. Sci. Anthr.*, 4, 000130,](#)
855 [<https://doi.org/10.12952/journal.elementa.000130>, 2016.](#)

856 Lee, K., Tong, L. T., Millero, F. J., Sabine, C. L., Dickson, A. G., Goyet, C., Park, G.-H., Wanninkhof, R., Feely,
857 R. A., and Key, R. M.: Global relationships of total alkalinity with salinity and temperature in surface waters of
858 the world's oceans, *Geophys. Res. Lett.*, 33, L19605, <https://doi.org/10.1029/2006GL027207>, 2006.

- Lueker, T. J., Dickson, A. G., and Keeling, C. D.: Ocean pCO₂ calculated from dissolved inorganic carbon, alkalinity, and equations for K₁ and K₂: validation based on laboratory measurements of CO₂ in gas and seawater at equilibrium, *Mar. Chem.*, 70, 105–119, [https://doi.org/10.1016/S0304-4203\(00\)00022-0](https://doi.org/10.1016/S0304-4203(00)00022-0), 2000.
- Mayot, N., Le Quéré, C., Rödenbeck, C., Bernardello, R., Bopp, L., Djeutchouang, L. M., Gehlen, M., Gregor, L., Gruber, N., Hauck, J., Iida, Y., Ilyina, T., Keeling, R. F., Landschützer, P., Manning, A. C., Patara, L., Resplandy, L., Schwinger, J., Séférian, R., Watson, A. J., Wright, R. M., and Zeng, J.: Climate-driven variability of the Southern Ocean CO₂ sink, *Philos. Trans. R. Soc. Math. Phys. Eng. Sci.*, 381, 20220055, <https://doi.org/10.1098/rsta.2022.0055>, 2023.
- McClish, S. and Bushinsky, S. M.: Majority of Southern Ocean Seasonal Sea Ice Zone Bloom Net Community Production Precedes Total Ice Retreat, *Geophys. Res. Lett.*, 50, e2023GL103459, <https://doi.org/10.1029/2023GL103459>, 2023.
- Meijers, A. J. S., Le Quéré, C., Monteiro, P. M. S., and Sallée, J.-B.: Heat and carbon uptake in the Southern Ocean: the state of the art and future priorities, *Philos. Trans. R. Soc. Math. Phys. Eng. Sci.*, 381, 20220071, <https://doi.org/10.1098/rsta.2022.0071>, 2023.
- Merlivat, L., Boutin, J., and d'Ovidio, F.: Carbon, oxygen and biological productivity in the Southern Ocean in and out the Kerguelen plume: CARIOCA drifter results, *Biogeosciences*, 12, 3513–3524, <https://doi.org/10.5194/bg-12-3513-2015>, 2015.
- [Merlivat, L., Hemming, M., Boutin, J., Antoine, D., Vellucci, V., Golbol, M., Lee, G. A., and Beaumont, L.: Physical mechanisms for biological carbon uptake during the onset of the spring phytoplankton bloom in the northwestern Mediterranean Sea \(BOUSSOLE site\), *Biogeosciences*, 19, 3911–3920, <https://doi.org/10.5194/bg-19-3911-2022>, 2022.](#)
- Mongwe, P., Gregor, L., Tjiputra, J., Hauck, J., Ito, T., Danek, C., Vichi, M., Thomalla, S., and Monteiro, P. M. S.: Projected poleward migration of the Southern Ocean CO₂ sink region under high emissions, *Commun. Earth Environ.*, 5, 1–13, <https://doi.org/10.1038/s43247-024-01382-y>, 2024.
- Naëck, K., Boutin, J., Beaumont, L., Lourenco, A., and Sallée, J.-B.: CARIOCA observations - SO-CHIC Cruise 2022, <https://doi.org/10.17882/100800>, 2024.
- Nicholson, S.-A., Whitt, D. B., Fer, I., Du Plessis, M. D., Lebéhot, A. D., Swart, S., Sutton, A. J., and Monteiro, P. M. S.: Storms drive outgassing of CO₂ in the subpolar Southern Ocean, *Nat. Commun.*, 13, 158, <https://doi.org/10.1038/s41467-021-27780-w>, 2022.
- OceanColour - CCI: <https://www.oceancolour.org/>, last access: 10 July 2024.
- Ogundare, M. O., Fransson, A., Chierici, M., Joubert, W. R., and Roychoudhury, A. N.: Variability of Sea-Air Carbon Dioxide Flux in Autumn Across the Weddell Gyre and Offshore Dronning Maud Land in the Southern Ocean, *Front. Mar. Sci.*, 7, 614263, <https://doi.org/10.3389/fmars.2020.614263>, 2021.
- OSCAR third degree resolution ocean surface currents | PO.DAAC / JPL / NASA: https://podaac.jpl.nasa.gov/dataset/OSCAR_L4_OC_third-deg, last access: 10 July 2024.
- Park, Y. -H., Park, T., Kim, T. -W., Lee, S. -H., Hong, C. -S., Lee, J. -H., Rio, M. -H., Pujol, M. -I., Ballarotta, M., Durand, I., and Provost, C.: Observations of the Antarctic Circumpolar Current Over the Udintsev Fracture Zone, the Narrowest Choke Point in the Southern Ocean, *J. Geophys. Res. Oceans*, 124, 4511–4528, <https://doi.org/10.1029/2019JC015024>, 2019.
- Pellichero, V., Boutin, J., Claustre, H., Merlivat, L., Sallée, J., and Blain, S.: Relaxation of Wind Stress Drives the Abrupt Onset of Biological Carbon Uptake in the Kerguelen Bloom: A Multisensor Approach, *Geophys. Res. Lett.*, 47, <https://doi.org/10.1029/2019GL085992>, 2020.
- Person, R., Aumont, O., Madec, G., Vancoppenolle, M., Bopp, L., and Merino, N.: Sensitivity of ocean biogeochemistry to the iron supply from the Antarctic Ice Sheet explored with a biogeochemical model, *Biogeosciences*, 16, 3583–3603, <https://doi.org/10.5194/bg-16-3583-2019>, 2019.

Person, R., Vancoppenolle, M., Aumont, O., and Malsang, M.: Continental and Sea Ice Iron Sources Fertilize the Southern Ocean in Synergy, *Geophys. Res. Lett.*, 48, e2021GL094761, <https://doi.org/10.1029/2021GL094761>, 2021.

Rousselet L., d'Ovidio F., Izard L., Della Penne A., Petrenko A., Barrillon S., Nencioli F., Doglioli A., (submitted, JTECH-D-240071), A Software Package for an Adaptive Satellite-based Sampling for Oceanographic cruises (SPASSOv2.0): tracking fine scale features for physical and biogeochemical studies, [\[2024 preprint\]](#).

Sabine, C. L., Feely, R. A., Gruber, N., Key, R. M., Lee, K., Bullister, J. L., Wanninkhof, R., Wong, C. S., Wallace, D. W. R., Tilbrook, B., Millero, F. J., Peng, T.-H., Kozyr, A., Ono, T., and Rios, A. F.: The Oceanic Sink for Anthropogenic CO₂, *Science*, 305, 367–371, <https://doi.org/10.1126/science.1097403>, 2004.

Sanial, V., van Beek, P., Lansard, B., d'Ovidio, F., Kestenare, E., Souhaut, M., Zhou, M., and Blain, S. (2014). Study of the phytoplankton plume dynamics off the Crozet Islands (Southern Ocean): A geochemical-physical coupled approach. *Journal of Geophysical Research: Oceans* 119, 2227–2237.

Sarmiento, J. L., Johnson, K. S., Arteaga, L. A., Bushinsky, S. M., Cullen, H. M., Gray, A. R., Hotinski, R. M., Maurer, T. L., Mazloff, M. R., Riser, S. C., Russell, J. L., Schofield, O. M., and Talley, L. D.: The Southern Ocean carbon and climate observations and modeling (SOCCOM) project: A review, *Prog. Oceanogr.*, 219, 103130, <https://doi.org/10.1016/j.pocean.2023.103130>, 2023.

~~Steiger, N., Sallée, J., Ward, B., Azevedo, A., Binase, Z., Ten Doeschat, A., Els, H., Hamnea, S., Jacobs, L., Katsoulis, M., Lavanchy, S., Lavis, C., Lourenco, A., Du Plessis, M., Rosenthal, H., Soares, B., and Spira, T.: CTD observation – SO-CHIC Cruise 2022, <https://doi.org/10.17882/95314>, 2022.~~

Sergi, S., Baudena, A., Cotté, C., Ardyna, M., Blain, S., and d'Ovidio, F.: Interaction of the Antarctic Circumpolar Current With Seamounts Fuels Moderate Blooms but Vast Foraging Grounds for Multiple Marine Predators, *Front. Mar. Sci.*, 7, 416, <https://doi.org/10.3389/fmars.2020.00416>, 2020.

Smith, R. M. and Bigg, G. R.: Impact of Giant Iceberg A68A on the Physical Conditions of the Surface South Atlantic, Derived Using Remote Sensing, *Geophys. Res. Lett.*, 50, e2023GL104028, <https://doi.org/10.1029/2023GL104028>, 2023.

~~Steiger, N., Sallée, J., Ward, B., Azevedo, A., Binase, Z., Ten Doeschat, A., Els, H., Hamnea, S., Jacobs, L., Katsoulis, M., Lavanchy, S., Lavis, C., Lourenco, A., Du Plessis, M., Rosenthal, H., Soares, B., and Spira, T.: CTD observation - SO-CHIC Cruise 2022, <https://doi.org/10.17882/95314>, 2022.~~

Sutherland, G., G. Reverdin, L. Marié, and B. Ward (2014), Mixed and mixing layer depths in the ocean surface boundary layer under conditions of diurnal stratification, *Geophys. Res. Lett.*, 41, doi:10.1002/2014GL061939.

Sutton, A. J., Williams, N. L., and Tilbrook, B.: Constraining Southern Ocean CO₂ Flux Uncertainty Using Uncrewed Surface Vehicle Observations, *Geophys. Res. Lett.*, 48, <https://doi.org/10.1029/2020GL091748>, 2021.

Swart, S., du Plessis, M., Giddy, I., Edholm, J., Spira, T., Biddle, L., and Rosenthal, H. S.: Dataset from autonomous assets collected during the SO-CHIC field campaign in the Southern Ocean (1), <https://doi.org/10.5281/ZENODO.11059425>, 2024.

Szekely, T., Gourrion, J., Pouliquen, S., and Reverdin, G.: CORA, Coriolis Ocean Dataset for Reanalysis, <https://doi.org/10.17882/46219>, 2024.

Takahashi, T., Sutherland, S. C., Sweeney, C., Poisson, A., Metzl, N., Tilbrook, B., Bates, N., Wanninkhof, R., Feely, R. A., Sabine, C., Olafsson, J., and Nojiri, Y.: Global sea–air CO₂ flux based on climatological surface ocean pCO₂, and seasonal biological and temperature effects, *Deep Sea Res. Part II Top. Stud. Oceanogr.*, 49, 1601–1622, [https://doi.org/10.1016/S0967-0645\(02\)00003-6](https://doi.org/10.1016/S0967-0645(02)00003-6), 2002.

Takahashi, T., Sweeney, C., Hales, B., Chipman, D. W., Newberger, T., Goddard, J. G., Iannuzzi, R. A., and Sutherland, S. C.: The Changing Carbon Cycle in the Southern Ocean, *Oceanography*, 25, 26–37, 2012.

The SO-CHIC consortium, Sallée, J. B., Abrahamsen, E. P., Allaigre, C., Auger, M., Ayres, H., Badhe, R., Boutin, J., Brearley, J. A., De Lavergne, C., Ten Doeschate, A. M. M., Droste, E. S., Du Plessis, M. D., Ferreira, D., Giddy, I. S., Gülk, B., Gruber, N., Hague, M., Hoppema, M., Josey, S. A., Kanzow, T., Kimmritz, M., Lindeman, M. R., Llanillo, P. J., Lucas, N. S., Madec, G., Marshall, D. P., Meijers, A. J. S., Meredith, M. P., Mohrmann, M.,

952 Monteiro, P. M. S., Mosneron Dupin, C., Naeck, K., Narayanan, A., Naveira Garabato, A. C., Nicholson, S.-A.,
 953 Novellino, A., Ödalen, M., Østerhus, S., Park, W., Patmore, R. D., Piedagnel, E., Roquet, F., Rosenthal, H. S.,
 954 Roy, T., Saurabh, R., Silvy, Y., Spira, T., Steiger, N., Styles, A. F., Swart, S., Vogt, L., Ward, B., and Zhou, S.:
 955 Southern ocean carbon and heat impact on climate, *Philos. Trans. R. Soc. Math. Phys. Eng. Sci.*, 381, 20220056,
 956 <https://doi.org/10.1098/rsta.2022.0056>, 2023.

957 Thomalla, S. J., Moutier, W., Ryan-Keogh, T. J., Gregor, L., and Schütt, J.: An optimized method for correcting
 958 fluorescence quenching using optical backscattering on autonomous platforms: Method for correcting fluorescence
 959 quenching, *Limnol. Oceanogr. Methods*, 16, 132–144, <https://doi.org/10.1002/lom3.10234>, 2018.

960 Vernet, M., Geibert, W., Hoppema, M., Brown, P. J., Haas, C., Hellmer, H. H., Jokat, W., Jullion, L., Mazloff, M.,
 961 Bakker, D. C. E., Brearley, J. A., Croot, P., Hattermann, T., Hauck, J., Hillenbrand, C. -D., Hoppe, C. J. M., Huhn,
 962 O., Koch, B. P., Lechtenfeld, O. J., Meredith, M. P., Naveira Garabato, A. C., Nöthig, E. -M., Peeken, I., Rutgers
 963 Van Der Loeff, M. M., Schmidtke, S., Schröder, M., Strass, V. H., Torres-Valdés, S., and Verdy, A.: The Weddell
 964 Gyre, Southern Ocean: Present Knowledge and Future Challenges, *Rev. Geophys.*, 57, 623–708,
 965 <https://doi.org/10.1029/2018RG000604>, 2019.

966 Wang, J., Luo, H., Yang, Q., Liu, J., Yu, L., Shi, Q., and Han, B.: An Unprecedented Record Low Antarctic Sea-
 967 ice Extent during Austral Summer 2022, *Adv. Atmospheric Sci.*, 39, 1591–1597, [https://doi.org/10.1007/s00376-](https://doi.org/10.1007/s00376-022-2087-1)
 968 022-2087-1, 2022.

969 Wanninkhof, R.: Relationship between wind speed and gas exchange over the ocean, *J. Geophys. Res.*, 97, 7373,
 970 <https://doi.org/10.1029/92JC00188>, 1992.

971 Wanninkhof, R.: Relationship between wind speed and gas exchange over the ocean revisited: Gas exchange and
 972 wind speed over the ocean, *Limnol. Oceanogr. Methods*, 12, 351–362, <https://doi.org/10.4319/lom.2014.12.351>,
 973 2014.

974 Ward, B., Azevedo, A., Binase, Z., ten Doeschate, A., Els, H., Hamnca, S., Jacobs, L., Katsoulis, M., Lavanchy,
 975 S., Lavis, C., Lourenco, A., du Plessis, M., Rosenthal, H., Sallee, J.-B., Soares, B., Spira, T., and Steiger, N.:
 976 SOCHIC cruise report, Zenodo, <https://doi.org/10.5281/ZENODO.6948850>, 2022.

977 Ward, B., Naëck, K., Boutin, J., Sallée, J.-B., Jacobs, L., and Steiger, N.: TSG observations - SO-CHIC Cruise
 978 2022, <https://doi.org/10.17882/100905>, 2024.

979 Weiss, R. F.: Carbon dioxide in water and seawater: the solubility of a non-ideal gas, *Mar. Chem.*, 2, 203–215,
 980 [https://doi.org/10.1016/0304-4203\(74\)90015-2](https://doi.org/10.1016/0304-4203(74)90015-2), 1974.